Fully quantum calculations of the line-shape parameters for the Hartmann-Tran profile: a CO-Ar case study

Grzegorz Kowzan, Piotr Wcislo, Michal Slowiński, Piotr Maslowski, Alexandra Viel, Franck. Thibault

Journal of Quantitative Spectroscopy & Radiative Transfer 243 (2020) 106803

Contents lists available at ScienceDirect

Journal of Quantitative Spectroscopy & Radiative Transfer

journal homepage: www.elsevier.com/locate/jqsrt

Fully quantum calculations of the line-shape parameters for the Hartmann-Tran profile: A CO-Ar case study

Grzegorz Kowzan[a,*], Piotr Wcisło[a], Michał Słowiński[a], Piotr Masłowski[a], Alexandra Viel[b], Franck Thibault[b]

[a] Institute of Physics, Faculty of Physics, Astronomy and Informatics, Nicolaus Copernicus University in Toruń, ul. Grudziądzka 5, 87–100 Toruń, Poland
[b] Univ Rennes, CNRS, IPR (Institut de Physique de Rennes)-UMR 6251, Rennes F-35000, France

ARTICLE INFO

Article history:
Received 9 October 2019
Revised 15 December 2019
Accepted 16 December 2019
Available online 18 December 2019

Keywords:
Hartmann-Tran profile
Databases
Molecular collisions
Spectral line shapes

ABSTRACT

We present a procedure for generating the parameters of the Hartmann-Tran profile (HTP) from purely first principles calculations. Starting from an absorber-perturber interaction potential, we calculate *S*-matrices describing the effect of collisions on the absorbing molecule. We then use the generalized Hess method to calculate speed-dependent pressure shift and broadening parameters, and the complex Dicke parameter, ν_{opt}, which accounts for such effects as the Dicke effect and correlations between dephasing and velocity-changing collisions. Based on these *ab initio* results, we derive the Hartmann-Tran profile parameters and evaluate the validity of the quadratic approximation of speed dependence and the hard-collision model of velocity-changing collisions adopted in the Hartmann-Tran profile. We also discuss the interpretation and speed dependence of ν_{opt}. Finally, we evaluate the approximation scheme for temperature dependence of HTP line-shape parameters adopted in the 2016 edition of the HITRAN database.

1. Introduction

The availability of accurate line-shape parameters, including the ones accounting for speed-dependent effects [1–3] and velocity-changing collisions [4], combined with an appropriate line-shape model permitting efficient evaluation of molecular line shapes are crucial for faithful reconstruction and interpretation of accurate molecular spectra [5–9] and for reduction of model-induced errors in atmospheric measurements of the Earth and other planets [10]. Various beyond-Voigt profiles [2,11–17] have been successfully used in analysis of molecular spectra exhibiting influence of speed dependence of broadening and shift as well as the influence of the Dicke effect, but their complexity and high computational cost made them unsuitable for use beyond interpretation of laboratory spectra. Since then, it was shown that the computational cost of a class of such profiles can be significantly lowered by employing the quadratic approximation of speed dependence [18–20], reducing it to at most five times that of the Voigt profile. The Hartmann-Tran profile utilizes this development and encompasses several beyond-Voigt profiles, allowing for fast and accurate line-shape modeling. This led to its recommendation by the IUPAC [21] and its adoption in the 2016 edition of the HITRAN database [22].

The HTP is described by the Doppler width of the transition and six collisional parameters. The 2016 edition of the HITRAN database allows for inclusion of the values of four of them at four reference temperatures corresponding to different temperature ranges. Of the remaining two, the correlation parameter is assumed to be temperature independent and the frequency of velocity-changing collisions is provided at a single temperature and described by a single power law for all temperature ranges. For two parameters, pressure broadening half-width and pressure shift, and for each temperature range, the temperature dependence coefficients also have to be provided. The parameters introduced into the database should primarily allow for accurate modeling of measured spectra in a wide temperature range. The task of filling the database with experimentally determined values of these parameters is made difficult by high demands on signal-to-noise ratio of the spectra, imperfections of the line-shape model and strong numerical correlation between fitted parameters [20,21,23]. An alternate approach to the technically difficult and time-consuming measurements was recently proposed by Ngo and Hartmann [24]. It combines requantized classical molecular dynamics simulations (rCMDS) and currently available measurements of pressure broadening halfwidths to generate a subset of HTP parameters. Here, we

* Corresponding author.
E-mail address: gkowzan@fizyka.umk.pl (G. Kowzan).

https://doi.org/10.1016/j.jqsrt.2019.106803

validate a method of obtaining *all* the HTP parameters from purely *ab initio* quantum-mechanical calculations.

Pressure broadening and shift parameters based on *ab initio* quantum-mechanical calculations have already been obtained for a number of systems [25,26], including CO-Ar [27–30]. In contrast, the complex Dicke parameter [31] ν_{opt}, has so far been only obtained in this manner for the hydrogen molecule isotopologues in helium baths [32–34] and D_2-D_2 [35], which are not representative of most systems relevant to atmospheric studies. Here, we derive a complete set of HTP parameters from *ab initio* calculations for the first time for an atmospherically relevant system, namely CO-Ar.

More specifically, we apply this approach to the two P(2) and P(8) CO-Ar fundamental band lines. We calculate pressure broadening and shift coefficients, and the complex Dicke parameter for a broad temperature range and provide thermally-averaged and quadratic-speed-dependent values of these parameters directly applicable to evaluation of the HTP. We establish the accuracy of the obtained pressure broadening and shift values by comparing them with the most accurate experimental values available, measured by Luo et al. [27] and Wehr et al. [30]. Further, we investigate the validity of the HTP approximations in several ways. First, we evaluate the model of velocity-changing collisions assumed in the HTP by comparing the HTP line shapes with the speed-dependent billiard ball profile (SDBBP) [36]. Second, we evaluate the quadratic approximation of the speed dependence of broadening and shift by directly comparing the *ab initio* and quadratic speed dependence of the parameters and by comparing the HTP line shapes calculated with *ab initio* and approximate speed dependence. Third, we examine the speed dependence of ν_{opt} and the consequences of including it in the HTP. We also validate a procedure for obtaining quadratic-speed-dependent parameters from otherwise known temperature dependence of thermally-averaged parameters [37,38].

The theoretical framework is described in Section 2. The CO-Ar results are gathered in Section 3. Tests of validity of various approximations are presented in Section 4 before Section 5 that concludes.

2. Theoretical framework

The HTP is described by a set of seven parameters:

$$\mathrm{HTP}(\Gamma_D, \Gamma_0, \Delta_0, \Gamma_2, \Delta_2, \nu_{\mathrm{VC}}, \eta; \Delta\nu), \tag{1}$$

where Γ_D is the Doppler half-width, Γ_0 is the pressure-broadened half-width at half-maximum (HWHM), Δ_0 is the pressure shift, Γ_2 and Δ_2 are the quadratic-speed-dependent pressure broadening and shift, ν_{VC} is the frequency of velocity-changing collisions and η is the correlation parameter. The argument, $\Delta\nu$, of the function is the detuning from the transition frequency. The pressure-independent equivalents of the five pressure-dependent parameters are defined as: $\gamma_0 = \Gamma_0/p$, $\delta_0 = \Delta_0/p$, $\gamma_2 = \Gamma_2/p$, $\delta_2 = \Delta_2/p$ and $\tilde{\nu}_{\mathrm{VC}} = \nu_{\mathrm{VC}}/p$.

The HTP is otherwise known as partially-correlated quadratic-speed-dependent hard-collision profile. The hard-collision profiles are usually derived by solving the classical Boltzmann transport-relaxation equation for the distribution function $f(\boldsymbol{r}, \boldsymbol{v_1}, t)$ of the active molecule [13,39]. The arguments of the function are: the position $\boldsymbol{r}$ and velocity $\boldsymbol{v_1}$ of the active molecule, and time t. The spectral line shape profile is obtained from the distribution function through the Fourier-Laplace transform. The solution of the Boltzmann equation is determined by the collision operator, which is separated into two terms: a first one, corresponding to dephasing collisions [40], responsible for pressure broadening and shift, and a second one, corresponding to combined velocity-changing and dephasing collisions. This description results in the general shape of the resonances which is specialized to a particular absorber-perturber pair by the speed-dependent pressure broadening and shift functions, $\Gamma(v_1)$ and $\Delta(v_1)$, the frequency of velocity-changing collisions, ν_{VC}, and the degree of correlation between those, through η. These four parameters are determined by the nature of absorber-perturber collisions, and provide a way to introduce precise *ab initio* quantum scattering calculations into the determination of line shapes.

2.1. Broadening, shift and their dependence on speed

Since the seminal works of Baranger [41–43], Fano [44] and Ben-Reuven [45,46] the formulas for spectroscopic cross sections are well known. They rely on expressing spectral lines as Liouville space elements and pressure broadening and shift coefficients as diagonal matrix elements of the relaxation operator in the line basis. For a diatomic molecule of mass m_1 perturbed by an atom of mass m_2 such elements are proportional to generalized cross sections given by:

$$\begin{aligned}\sigma^q_{\lambda=0}(\nu_a, j_a, \nu_b, j_b; E_{\mathrm{kin}}) = \frac{\pi}{k^2} \sum_{J_a J_b, l, l'} [J_a][J_b](-1)^{l-l'} \\ \times \begin{Bmatrix} j_a & q & j_b \\ J_b & l & J_a \end{Bmatrix} \begin{Bmatrix} j_a & q & j_b \\ J_b & l' & J_a \end{Bmatrix} \\ \times \left(\delta_{ll'} - S^{*J_b}(\nu_b, j_b, l'; \nu_b, j_b, l) S^{J_a}(\nu_a, j_a, l'; \nu_a, j_a, l)\right),\end{aligned} \tag{2}$$

where J_a, J_b are total angular momenta, l, l' are orbital angular momenta and ν_a, j_a, ν_b, j_b are initial and final rovibrational quantum numbers of the diatomic before and after the optical transition. $\{: : :\}$ is the 6-j symbol, $[x]$ stands for $(2x+1)$, q denotes the tensor order of the optical transition and λ denotes the rank of the molecular velocity tensor associated with the cross section. For electric dipole transitions considered in this article $q = 1$ and for the dephasing cross section $\lambda = 0$. S-matrix elements are expressed in the total angular momentum coupling scheme for fixed kinetic energy E_{kin}. The magnitude of the wavevector $\boldsymbol{k}$ is determined by the relative center-of-mass kinetic energy $k^2 = 2\mu E_{\mathrm{kin}}/\hbar^2$, where $\mu = m_1 m_2/(m_1 + m_2)$ is the reduced mass of the system. Subsequently, the j and ν indices will be omitted for brevity. Similarly, all the HTP line-shape parameters, Eq. (1), are implicit functions of temperature T, through energy dependence of $\sigma^q_\lambda(E_{\mathrm{kin}})$ averaged over Maxwell–Boltzmann distribution, but in the following the argument T will be omitted, *e.g.* $\Gamma_0 \equiv \Gamma_0(T)$. The formulas are given for line-shape parameters expressed in units of angular frequency. The thermally-averaged parameters at a given concentration of the perturbing atom, n, are obtained from the following expression [47,48]:

$$\Gamma_0 - \imath\Delta_0 = n\langle v_r\rangle\langle\sigma^q_{\lambda=0}(E_{\mathrm{kin}} = \mu v_r^2/2)\rangle, \tag{3}$$

where $\langle v_r\rangle = \sqrt{8k_BT/\pi\mu}$ is the mean relative speed and $\langle\dots\rangle$ denotes integration over the Maxwell–Boltzmann energy distribution,

$$\langle\sigma^q_{\lambda=0}(E_{\mathrm{kin}})\rangle = \left(\frac{1}{k_BT}\right)^2 \int_0^\infty E_{\mathrm{kin}}\sigma^q_{\lambda=0}(E_{\mathrm{kin}}) e^{-\frac{E_{\mathrm{kin}}}{k_BT}}\,\mathrm{d}E_{\mathrm{kin}}. \tag{4}$$

The speed-dependent parameters are obtained by averaging the cross sections over the distribution function $f(v_r|v_1)$ of relative velocity v_r with respect to the absorber velocity v_1 at a given T [49]:

$$\Gamma(v_1) - \imath\Delta(v_1) = n\int_0^\infty v_r\sigma^q_{\lambda=0}\left(E_{\mathrm{kin}} = \mu v_r^2/2\right) f(v_r|v_1)\,\mathrm{d}v_r. \tag{5}$$

The obtained *ab initio* parameters are used to determine the quadratic-speed-dependent parameters (see Eq. (A.7)), Γ_2, Δ_2, by requiring the derivatives of both *ab initio* and quadratic speed dependence to be equal at the most probable speed of the active

molecule $v_p = \sqrt{2k_BT/m_1}$, hence:

$$\Gamma_2 = \frac{v_p}{2}\frac{\mathrm{d}}{\mathrm{d}v}\Gamma(v_1)\bigg|_{v_1=v_p}. \tag{6}$$

2.2. The complex Dicke parameter

In the framework of the classical Boltzmann equation the physics of velocity-changing collisions and their effect on the line shape is encapsulated in the probability rate $A(\boldsymbol{v_1'}, \boldsymbol{v_1})$, describing the probability per unit time for velocity change $\boldsymbol{v_1'} \to \boldsymbol{v_1}$ of the absorber to occur. In order to obtain a closed-form solution, permitting fast evaluation of the line shape, a simplifying assumption is made. It assumes that the effect of a collision is independent of the initial collision velocity and that the final velocity is determined only by the frequency of velocity-changing collisions ν_{VC} and the equilibrium velocity distribution $f_{\mathrm{MB}}(\boldsymbol{v_1})$, *i.e.*, $A(\boldsymbol{v_1'}, \boldsymbol{v_1}) = \nu_{\mathrm{VC}} f_{\mathrm{MB}}(\boldsymbol{v_1})$; this assumption leads to the familiar hard-collision model.

The separate treatment of confinement narrowing, collisional broadening and shift depends on the assumption that the associated velocity-changing and dephasing collisions occur independently. If velocity-changing collisions are correlated with dephasing collisions, then the ν_{VC} frequency is replaced by the ν_{opt} frequency which is in general smaller than ν_{VC}. The reason for this substitution is that the ν_{VC} frequency includes velocity changes of the part of optical coherence which was damped (or phase-shifted) by dephasing collisions. The HTP's hard collision model takes into account this effect by defining ν_{opt} as

$$\nu_{\mathrm{opt}}^{\mathrm{HTP}}(v_1) = \nu_{\mathrm{VC}} - \eta[\Gamma(v_1) + \imath\Delta(v_1)]. \tag{7}$$

In Eq. (7), η is a phenomenological correlation parameter and ν_{VC} is the constant frequency of velocity-changing collisions from the uncorrelated model. The imaginary part of ν_{opt} leads to an asymmetry of the profile distinct from the asymmetry caused by the speed dependence of pressure shift.

Similarly to pressure broadening and shift coefficients, the complex Dicke parameter, ν_{opt}, can be calculated from first principles, provided an accurate interaction potential is available. The theory of Hess [50,51] connects the developments of Baranger [41–43], Fano [44] and Ben-Reuven [45,46] with the quantum treatment of transport-relaxation phenomena [52,53]. In the resultant quantum Boltzmann-like kinetic equation the effect of correlated velocity-changing and dephasing collisions on the line shape is explicitly included and described in terms of the flow of the spectral transition operator through the gas. Within the generalized Hess method (GHM) [54], this leads to a definition of the cross section for velocity change of an optical coherence. A formula for this cross section in terms of S-matrix elements and in the case of an isolated line of a diatomic molecule perturbed by an atom is provided below [54–57]:

$$\begin{aligned}\sigma^q_{\lambda=1}(\nu_a, j_a, \nu_b, j_b; E) = \frac{\pi}{k^2} \sum_{\substack{J_a J_b \\ l_a, l_a', l_b, l_b'}} [J_a][J_b]\sqrt{[l_a][l_a'][l_b][l_b']} \\ \times \begin{pmatrix} l_a & l_b & \lambda \\ 0 & 0 & 0 \end{pmatrix} \begin{pmatrix} l_a' & l_b' & \lambda \\ 0 & 0 & 0 \end{pmatrix} \begin{bmatrix} j_a & j_a & l_b & l_b' \\ j_b & l_a & j_b & l_a' \\ q & J_b & J_a & \lambda \end{bmatrix} \\ \times \imath^{l_a' - l_a + l_b' - l_b} \Big(\delta_{l_a l_a'} \delta_{l_b l_b'} - S^{*J_b}(\nu_b, j_b, l_b'; \nu_b, j_b, l_b) \\ \times S^{J_a}(\nu_a; j_a, l_a'; \nu_a, j_a, l_a) \Big),\end{aligned} \tag{8}$$

the same notation as in Eq. (2) is used. In addition, (: : :) refers to the 3-j symbol and [: : : : : :] to the 12-j symbol of the second kind [58]. Introducing the collision integrals, $\omega_\lambda^{s,s'}(q)$, as being the thermally averaged cross sections [56,57]:

$$\omega_\lambda^{s,s'}(q) = \langle v_r \rangle \int_0^\infty x^{(s+s'+2)/2} e^{-x} \sigma_\lambda^q(E_{\mathrm{kin}} = x k_B T)\, \mathrm{d}x, \tag{9}$$

the thermally-averaged frequency ν_{opt} is defined by

$$\nu_{\mathrm{opt}}^{\mathrm{GHM}} = nM_2\left[\frac{2}{3}\omega_1^{11}(q)^* - \omega_0^{00}(q)^*\right], \tag{10}$$

with $M_i = m_i/(m_1 + m_2)$. Clearly, for $s = s' = 0$ and $\lambda = 0$ we retrieve the results from the earlier theories and $n\omega_0^{00}(q) = \Gamma_0 - \imath\Delta_0$, see Eq. (3).

The form of ν_{opt} assumed by the HTP, Eq. (7), is different from the one in the GHM, Eq. (10). Eq. (7) defines ν_{opt} as a function of absorber's speed and restricts ν_{VC} to real values. We obtain the values of ν_{VC} and η by requiring the thermally-averaged value of $\nu_{\mathrm{opt}}^{\mathrm{HTP}}(v_1)$ to be equal to $\nu_{\mathrm{opt}}^{\mathrm{GHM}}$, which implies the following relations:

$$\nu_{\mathrm{VC}} = \mathrm{Re}\,\nu_{\mathrm{opt}}^{\mathrm{GHM}} + \eta\Gamma_0, \tag{11}$$

$$\eta = -\frac{\mathrm{Im}\,\nu_{\mathrm{opt}}^{\mathrm{GHM}}}{\Delta_0}. \tag{12}$$

Together with the speed-dependent broadening $\Gamma(v_1)$ and shift $\Delta(v_1)$, obtained according to Eq. (5), this indirect identification of the HTP parameters, ν_{VC} and η, enables evaluation of the HTP based on quantum mechanical calculations.

3. Results for Ar-perturbed CO lines

Ab initio calculations of spectroscopic cross sections require a potential describing the interaction between the active molecule and the perturber molecule. In the case of CO and Ar, *i.e.* a diatomic molecule and a structureless atom, the interaction potential is expressed as a function of the distance R between the CO center of mass and the Ar atom, the distance r between C and O atoms, and the angle θ between the corresponding vectors $\boldsymbol{R}$ and $\boldsymbol{r}$. In the current calculations, we used the potential of Sumiyoshi and Endo [59], which was expanded in the basis of Legendre polynomials [60] up to 10th order. The extent of values for the CO bond length determined in [59], namely 1.0 to 1.35 Å, covered 99.98% of the squared wave function amplitude of the upper vibrational state (for a non-rotating, $j = 0$, CO), which from our experience can be considered as sufficient for accurate calculations of $\nu = 0 \to 1$ transitions.

The S-matrix calculations were performed with the MOLSCAT code [61] and its implementation of the modified log-derivative propagator [62,63]. The grid of collision energies at which S-matrices were calculated was limited to 1700 cm^{-1} [64] and its density was adjusted to obtain smooth σ_λ^q curves, with denser sampling at low collision energies and sparser sampling at high collision energies. Fig. 1 shows the spectroscopic cross sections for the P(2) and P(8) lines with insets for collision energies below the potential well depth *i.e.* below 107.1 cm^{-1}. A power-law dependence was used to fit cross sections, see Eq. (A.4), ignoring low-energy points. For $\mathrm{Re}(\sigma_0^1)$, $\mathrm{Re}(\sigma_1^1)$ the cut off was set at 50 cm^{-1}, for $\mathrm{Im}(\sigma_0^1)$ it was set at 100 cm^{-1}, and for $\mathrm{Im}(\sigma_1^1)$ at 200 cm^{-1}. The cut offs for the fits of the real parts of cross sections were set to ignore low-energy points because they do not contribute significantly to Boltzmann integrals, Eqs. (4), (9), at most temperatures accessible to experiment and cause the fits to have different asymptotic limits than the *ab initio* data. For the imaginary parts of the cross sections, it was clear from visual inspection that the low-energy part could not be fitted well with a single power-law, therefore the limit was set even higher. The fitted values are provided in Table A.1 and were used for evaluation of hypergeometric

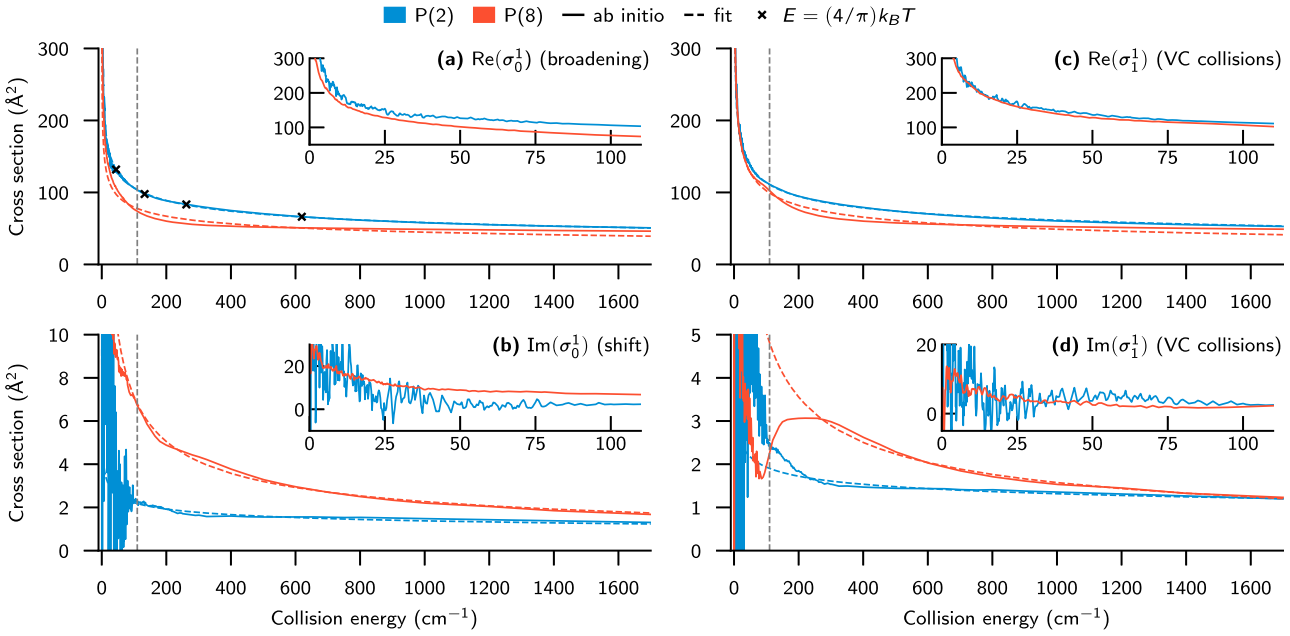

Fig. 1. Spectroscopic cross sections describing the effects of dephasing (a, b) and velocity-changing (c, d) collisions. Insets show the cross sections for collision energies below the potential well depth (107.1 cm^{-1}) and vertical dashed lines mark the well depth energy. The dashed lines show the fits of cross sections to power-law dependence from Eq. (A.4). The crosses in (a) mark the mean relative speed energies ($= \frac{4}{\pi}\frac{k_BT}{hc}$) corresponding to HITRAN reference temperatures: 50 K, 150 K, 296 K and 400 K.

speed dependence according to Eq. (A.6); all the other results presented in this paper are based on interpolated and extrapolated raw data, *i.e.* the solid lines in Fig. 1. The P(2) line cross sections at low collision energies exhibit strong signatures of Ar-CO resonances [65], which are much diminished for the P(8) line due to higher degree of centrifugal screening.

The cross sections were extrapolated to higher energies if necessary and interpolated with cubic B-splines, before performing the numerical integration of Eqs. (4), (5), (9). The upper limit of integration for thermal averaging at a given temperature, Eqs. (4), (9), was set by the 0.9999 quantile of $\langle x^2\exp(-x)\rangle$ distribution and the maximum absorber speed for which $\gamma(\nu_1; T)$ (and $\delta(\nu_1; T)$) was calculated was the 0.999 quantile of the Maxwell–Boltzmann speed distribution.

The calculations were carried out using the computer cluster of Institute of Physics of Rennes. The calculation time increases with increasing j_a value for a P(j_a) line due to increasing number of basis states. It amounts to a few hours for the P(2) line and up to a few days for, *e.g.* the P(14) line. The full determination of the line-shape parameters for all lines between rotational states populated at the considered temperatures would thus be in principle doable with only some more human time investment. However, since the purpose of the study is to demonstrate the general procedure and to investigate its broader implications, we restrict ourselves to the two P(2) and P(8) lines.

Table 1 presents the line-shape parameters obtained from *ab initio* calculations cast into parametrization of the HTP adopted in the 2016 edition of the HITRAN database. Pressure-independent HTP parameters, γ_0, δ_0, γ_2, δ_2, $\tilde{\nu}_{VC}$, were obtained in units of cm^{-1}/atm by evaluating Eqs. (3), (10) for $n = n_0(T_0/T)$ and multiplying the result by $(2\pi c)^{-1}$, where n_0 is the Loschmidt constant, $T_0 = 273.15$ K and c is the speed of light in vacuum. The parameters are provided at four temperatures, together with coefficients allowing to approximate them at other temperatures with a linear function: δ_0' (Eq. (A.2)), and with a power-law function: n_{γ_0} (Eq. (A.1)) and κ (Eq. (A.3)). The details of the approximation scheme are provided in Appendix A, following Ref. [38].

Table 1
HTP parameters of the P(2) and P(8) line within the parametrization adopted in the 2016 edition of HITRAN: γ_0, pressure half-width; n_{γ_0}, temperature depedence coefficient of γ_0; δ_0, pressure shift; δ', temperature dependence coefficient of δ_0; γ_2, speed-dependence of pressure half-width; δ_2, speed-dependence of pressure shift; $\tilde{\nu}_{VC}$, frequency of velocity-changing collisions; κ, temperature dependence coefficient of $\tilde{\nu}_{VC}$; η, correlation parameter. The parameters n_{γ_0}, κ and η are dimensionless. All the other parameters are expressed in 10^{-3} cm^{-1}/atm. The approximation scheme for temperature dependence of the parameters is described in Appendix A.

Line	Param.	T_{ref}			
		50 K	150 K	296 K	400 K
P(2)	γ_0	252.2	109.8	65.68	34.16
	n_{γ_0}	0.760	0.754	0.759	0.758
	γ_2	31.02	14.16	8.494	4.268
	δ_0	−8.61	−2.6	−1.48	−0.812
	δ'	0.105	0.0156	0.0035	0.00103
	δ_2	2.15	0.014	−0.14	−0.132
	$\tilde{\nu}_{VC}$	–	10.50	–	–
	κ	–	1.16	–	–
	η	–	−0.045	–	–
P(8)	γ_0	202.0	79.99	47.90	27.08
	n_{γ_0}	0.856	0.799	0.71	0.641
	γ_2	16.62	6.759	5.988	4.739
	δ_0	−18.4	−6.76	−3.55	−1.51
	δ'	0.19	0.043	0.0111	0.00297
	δ_2	−1.15	−0.318	−0.113	0.00305
	$\tilde{\nu}_{VC}$	–	36.46	–	–
	κ	–	0.861	–	–
	η	–	0.231	–	–

Fig. 2 shows the *ab initio* (solid line) and approximate values (dashed line) of the HTP parameters. For the P(8) line γ_0 values, the differences between *ab initio* and approximate values stay below 1% in the whole temperature range considered here. For the P(2) line the agreement is even better and discrepancies are not larger than 0.1%, except in the lowest temperature range, *i.e.* below 150 K. This can be seen to be consistent and indicative of how well the appropriate cross sections, see Fig. 1, themselves agree with the power-law dependence. The temperature dependence of γ_2 is

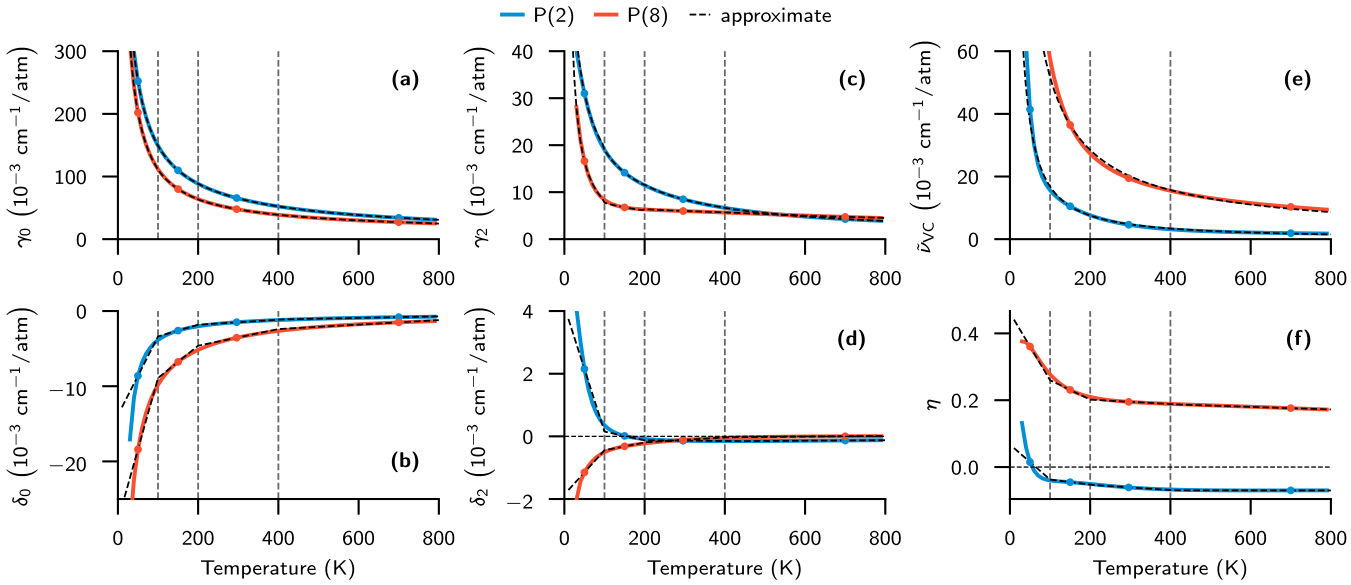

Fig. 2. Temperature dependence of pressure-independent line-shape parameters of P(2) and P(8) lines: (a) pressure half-width γ_0, (b) pressure shift δ_0, (c) speed-dependence of pressure half-width γ_2, (d) speed-dependence of pressure shift δ_2, (e) frequency of velocity-changing collisions $\tilde{\nu}_{VC}$, (f) correlation parameter η. The vertical dashed lines delimit the temperature ranges and the circles mark the line-shape parameters at the reference temperatures defined in the 2016 edition of the HITRAN database. The black dashed curves show the results of applying linear approximation, Eq. (A.2), in panels (b, d, f) and power-law approximation, Eqs. (A.1), (A.3), in panels (a, c, e). The horizontal dashed lines in (d) and (f) mark the zero level.

not explicitly included in the 2016 edition of the HITRAN database, with only the values at reference temperatures being given, but it can also be seen in Fig. 2c that it is well described by power-law dependence. The approximate γ_2 values match the *ab initio* values within 1% above 100 K for the P(2) line and above 200 K for the P(8) line, while at lower temperatures the discrepancies reach several percent for both lines. It should be noted at this point that the effect on the line shapes of these several-percent approximation errors of γ_2 is negligible compared to the effect of the quadratic approximation itself. We fitted $\tilde{\nu}_{VC}$ values to a power law with exponent κ in the whole temperature range based on the reference value of $\tilde{\nu}_{VC}$ evaluated at 150 K. The error of approximation is within 4% in the whole range for the P(2) line. For the P(8) line, the perfect agreement at the reference temperature worsens to 10% and 20% at higher and lower edges of temperature range, respectively. For both lines approximation errors of δ_0 stay below 10% and only increase beyond that value at temperatures below 100 K. For δ_2, the relative error between the full quantum and the approximation is not a relevant quantity to discuss as δ_2 is close (or even equal) to zero. The approximated and reference δ_2 values differences are however found to be small and the error made when using the approximation would have a negligible influence on the actual line shape.

The spectroscopic cross sections used in Fig. 1 and in all subsequent calculations are available in the supplementary material [dataset] [66]. Also included are the HTP parameters for temperatures from 30 K to 800 K in step of 10 K, *i.e.* the data for solid lines in Fig. 2, and the contents of Table 1.

We estimate the accuracy of the calculations by comparing our γ_0 and δ_0 values with the ones reported in [27,30]. Luo et al. [27] provided broadening and shift parameters for P and R branch transitions up to rotational level $j = 24$, whereas the overall more accurate results of Wehr et al. [30] are available only for P(j_a) lines with $j_a = 1, 2, 5, 7, 10, 13, 16$. Table 2 presents the comparison for the P(2) line at the experimental temperatures. The pressure broadening parameters γ_0 were found to all agree at sub-percent level, but for pressure shifts δ_0 the observed discrepancies were larger, reaching to about 3% for two of the considered temperatures. The shifts are in general considered more difficult to calculate accurately because of their higher sensitivity to the shape of the potential, slower convergence with total angular momentum J_{tot} and their lower absolute values. The last factor is especially important for the fundamental band transitions considered here, which are characterized by very weak pressure shifts. As an example of relatively slow convergence of $\mathrm{Im}(\sigma_0^1)$ with J_{tot}, at $E_{kin} = 300\ \mathrm{cm}^{-1}$ the required J_{tot} value for 1% accuracy was 328, but for $\mathrm{Re}(\sigma_0^1)$ it was only 109. Comparing the calculated pressure broadening of the P(8) line at 296 K equal to $47.90 \times 10^{-3}\ \mathrm{cm}^{-1}/\mathrm{atm}$ with the value of $46.96 \times 10^{-3}\ \mathrm{cm}^{-1}/\mathrm{atm}$ measured by Luo et al. [27], we see a discrepancy of 2%, which is to be expected considering that broadening of other transitions measured both by Luo et al. [27] and Wehr et al. [30] was found to be underestimated by the former by a similar amount. Because the variations in pressure shift of P-branch lines for j_a values between 7 to 13 are smaller than 1% [30], which is less than the disagreement between δ_0 values of Luo et al. [27] and Wehr et al. [30], we compare our value of P(8) line pressure shift of $-3.56 \times 10^{-3}\ \mathrm{cm}^{-1}/\mathrm{atm}$ with the pressure shift of the P(7) line from Ref. [30] equal to $-3.51 \times 10^{-3}\ \mathrm{cm}^{-1}/\mathrm{atm}$. The difference between these values is

Table 2
Comparison of pressure broadening γ_0 and shift δ_0 coefficients calculated in this work and measured by Wehr et al. [30] for the P(2) line. The values in the table are in $10^{-3}\ \mathrm{cm}^{-1}/\mathrm{atm}$ unless specified differently in the parentheses.

Param.	T (K)	Wehr	Calc.	Diff.	Diff. (%)
γ_0	323.9	60.99(5)	61.34	−0.35	−0.57
	294.5	65.33(3)	65.94	−0.61	−0.93
	258.7	72.53(5)	72.75	−0.22	−0.30
	236.4	77.81(4)	77.89	−0.08	−0.10
	214.1	83.89(5)	83.95	−0.06	−0.07
δ_0	323.8	−1.37(4)	−1.39	0.02	−1.38
	295.0	−1.46(2)	−1.49	0.03	−1.94
	258.7	−1.70(4)	−1.64	−0.06	3.24
	236.4	−1.82(3)	−1.77	−0.05	3.00
	214.0	−1.90(3)	−1.91	0.01	−0.68

−1.4%, which confirms the accuracy of our calculated pressure shift coefficient for the P(8) line.

4. Validity of the HTP approximations

4.1. Validity of the quadratic approximation

Fig. 3 shows the *ab initio* speed dependence of the line-shape parameters and their approximation (see Appendix A) with quadratic and hypergeometric functions at 296 K. The quadratic speed dependence was derived from *ab initio* dependence based on Eq. (6) and the hypergeometric speed dependence was obtained with Eq. (A.6) from power-law fits of spectroscopic cross sections shown in Fig. 1. As described in Appendix A, Eq. (A.4), different power-law dependencies of spectroscopic cross sections on collision energy give rise to different speed dependence of pressure broadening and shift. Quadratic speed dependence of $\Gamma(\nu_1)$, $\Delta(\nu_1)$ is associated with square-root energy dependence of cross sections, whereas hypergeometric speed dependence allows for an arbitrary exponent in power-law dependence. As evidenced by the fitted exponents provided in Table A.1, square-root law ($\alpha = 1/2$ in Eq. (A.4)) would fail at modeling the cross sections in Fig. 1. Hypergeometric model can be therefore expected to better account for speed dependence of broadening and shift. For the P(2) line broadening this improvement is confirmed, but for the P(8) line broadening the quadratic model better matches the *ab initio* data. For line shifts the situation is reverse. This shows that better physical justification of the power law [67] and more accurate modeling of $\sigma_\lambda^q(E)$ cross sections it offers, does not simply translate to improved performance of the hypergeometric model over the quadratic model. The work of Lance et al. [68] on C_2H_2-Xe line shapes and the recent developments by Gamache and Vispoel [69] suggest that a sum of hypergeometric functions or a higher order polynomial model would be required to unequivocally improve on the quadratic approximation. The level of disagreement between different models is quantified and summarized in Table 3.

Table 3
Integrated absolute-value percent differences between *ab inito*, quadratic (quad) and hypergeometric (hg) speed dependence. The residuals were weighted by Maxwell–Boltzmann speed distribution and divided by thermally-averaged values of the parameters at 296 K. All the values are given in percents.

Param.	P(2)		P(8)	
	quad	hg	quad	hg
γ	2.8	0.2	0.8	1.5
δ	0.8	3.0	1.7	1.6

In order to study the influence of the quadratic approximation on the line shapes, we have simulated several profiles, see Fig. 4. The three selected pressures – 10, 40 and 300 Torr – correspond to Γ_0/Γ_D ratios of about 0.13, 1.0, 3.9. The top panel shows the SDBBP with *ab initio* speed dependence (aiSDBBP), which we treat here as the reference line-shape model following its success in describing the line shapes of a variety of molecular systems, see references in [26], and CO-Ar in particular [29]. The remaining profiles are: HTP (qHTP), HTP with *ab initio* speed dependence (aiHTP) and SDBBP with quadratic speed dependence (qSDBBP). The top panel profiles and profile differences in lower panels are normalized to the peak value of aiSDDBP at each pressure. The lack of appreciable differences between aiHTP - aiSDBBP and qHTP - qSDBBP curves shows that the differences between quadratic and *ab initio* speed dependence are not large enough to affect the comparison between hard-collision and billiard ball model. That is to say, the effects of quadratic and hard-collision approximations are additive and considering them separately here is justified. The differences (qHTP−aiHTP) between the quadratic HTP and *ab initio* HTP obtained using the HTP in conjunction with Eqs. (5) and (6) exhibit the expected increase with increasing pressure and qualitatively

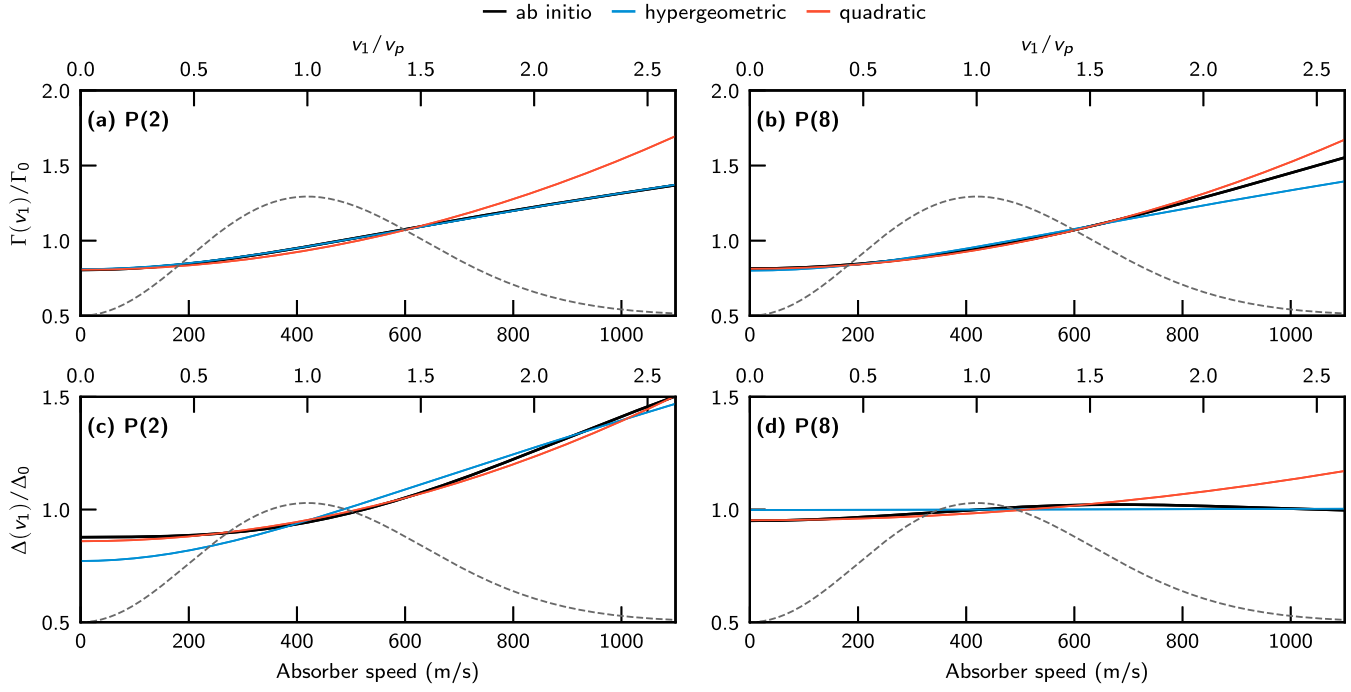

Fig. 3. Speed-dependent broadening and shift of P(2), (a, c), and P(8), (b, d), lines at 296 K. Black lines show the speed dependence obtained by evaluating Eq. (5) directly on the cross sections; blue lines show the hypergeometric speed dependence described by Eq. (A.6) evaluated with power-law fit coefficients from Table A.1; red lines show quadratic speed dependence described by Eq. (A.7) evaluated with coefficients obtained from Eq. (6). On panel (a) the black and blue curves overlap and are indistinguishable. Maxwell–Boltzmann speed distribution of CO at 296 K is shown as a dashed curve. (For interpretation of the references to colour in this figure legend, the reader is referred to the web version of this article.)

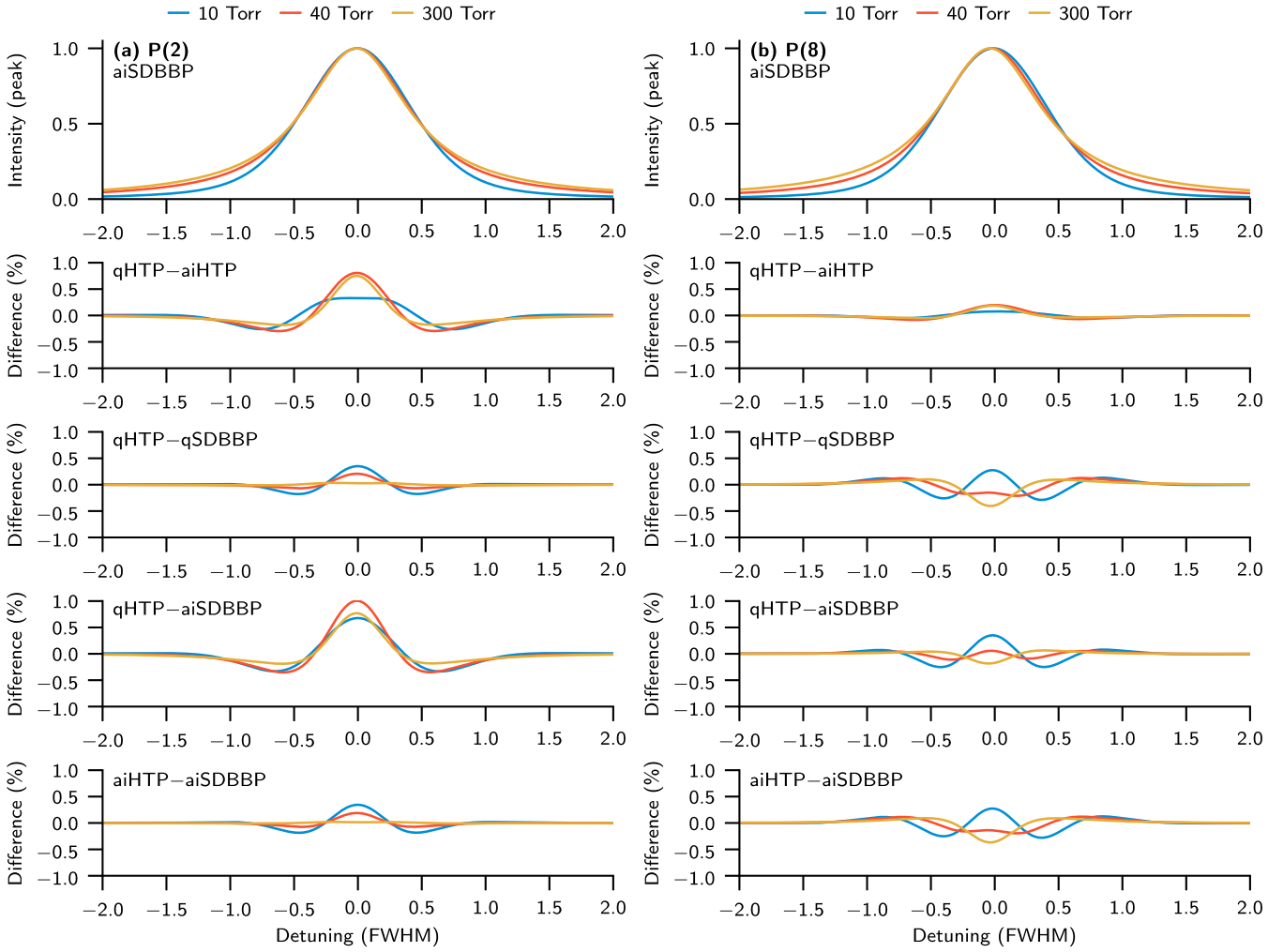

Fig. 4. P(2) line (left column) and P(8) line (right column) simulated line-shape profiles at 296 K. Top row shows the SDBBP with *ab initio* speed dependence (aiSDBBP) normalized to the peak value of the profile at each pressure. Lower rows show the differences between HTP (qHTP), HTP with substituted *ab initio* speed dependence (aiHTP), SDBBP with quadratic speed dependence (qSDBBP) and aiSDBBP. The differences between profiles were normalized by dividing them by the peak value of aiSDBBP profile at the same pressure. The frequency axis in each plot is in units of full-width at half-maximum (FWHM) of the aiSDBBP.

follow the results from Table 3; the P(8) line speed dependence is more faithfully modeled by quadratic speed dependence than the P(2) line. Notably, for the P(8) line the combined effect of quadratic and hard-collision approximations reduces the residuals relative to only hard-collision approximation, see the qHTP−aiSDBBP curve, showing strong correlation between Γ_2 and ν_{VC}. The accuracy of the quadratic approximation is on the order of a single percent, which is similar to the level of disagreement between hard-collision and billiard ball models (qHTP−qSDBBP). This shows that for these CO-Ar lines a more accurate description of both effects would be required for an overall better agreement with *ab initio* line shapes.

4.2. Validity of the approximation of the velocity-changing model

The HTP, GHM profile and SDBBP can all be derived by using the generalized Waldmann-Snider equation [50] to express the molecular line shape in terms of $\phi(\omega, \boldsymbol{v_1})$, the velocity distribution of the optical coherence associated with the transition:

$$f_{\mathrm{MB}}(\boldsymbol{v_1}) = \left[-\imath(\omega - \omega_0 - \boldsymbol{k}\cdot\boldsymbol{v_1}) - \hat{S}\right]\phi(\omega, \boldsymbol{v_1}), \tag{13}$$

where $f_{\mathrm{MB}}(\boldsymbol{v_1})$ is the equilibrium (Maxwell) velocity distribution, $\boldsymbol{k}\cdot\boldsymbol{v_1}$ describes the Doppler shift and ω, ω_0 are, respectively, the angular frequency of the incident radiation and of the transition. In both the uncorrelated hard-collision model and the SDBBP the collision operator is of the form:

$$\hat{S} = -\Gamma(v_1) - \imath\Delta(v_1) + \nu_{\mathrm{VC}}\hat{\mathrm{M}}, \tag{14}$$

where $\hat{\mathrm{M}} \equiv \hat{\mathrm{M}}_{\mathrm{BB}}$ is the hard-sphere kernel (billiard-ball kernel) for the SDBBP and $\hat{\mathrm{M}} \equiv \hat{\mathrm{M}}_{\mathrm{HC}}$ is the hard-collision kernel. Analogously to the correlated hard-collision model, see Section 2.2, the influence of velocity-changing and dephasing collisions can be taken into account in the billiard ball model by substituting ν_{VC} with ν_{opt}. In this case, both the SDBBP and HTP collision operator can be expressed as:

$$\hat{S} = -\Gamma(v_1) - \imath\Delta(v_1) + \nu_{\mathrm{opt}}\hat{\mathrm{M}}. \tag{15}$$

In the GHM, the collision operator is given by:

$$\hat{S}\phi(\omega, \boldsymbol{v_1}) = -\omega_A\langle\phi(\omega, \boldsymbol{v_1})\rangle - \omega_R[\phi(\omega, \boldsymbol{v_1}) - \langle\phi(\omega, \boldsymbol{v_1})\rangle], \tag{16}$$

where $\langle\ldots\rangle$ denotes integration over $f_{\mathrm{MB}}(\boldsymbol{v_1})$, $\omega_A = \Gamma_0 + \imath\Delta_0$ and ω_R is a complex coefficient chosen to minimize the error of approximating the collision operator by only two complex numbers. In order to obtain a closed-form formula for ω_R, the coefficient is expanded in powers of $\boldsymbol{k}\cdot\boldsymbol{v_1}$ and the expansion is truncated to retain only the first-order term in $\boldsymbol{k}$. This leads to identification of ω_R with the collision integral for the flow of optical coherence, which

in terms of $\omega_0^{00}(q)$ and $\omega_1^{11}(q)$, Eq. (9), is given by:

$$\omega_R = n\left[\frac{2}{3}M_2\omega_1^{11}(q)^* + M_1\omega_0^{00}(q)^*\right]. \tag{17}$$

Reducing ω_R to a term linear in concentration also results in a closed-form solution of Eq. (13) with the GHM collision operator, Eq. (16). The GHM line-shape profile is formally equivalent [32] to speed-independent HTP, *i.e.* correlated Rautian-Sobel'man profile. With $\nu_{\text{opt}}^{\text{GHM}}$ defined as $\nu_{\text{opt}}^{\text{GHM}} = \omega_R - \omega_A$, leading to Eq. (10), this equivalence allowed us to identify the GHM line-shape parameters with Γ_0, Δ_0 and ν_{opt} parameters and express in their terms the ν_{VC} and η parameters used in the HTP, Eqs. (11), (12). Using the same $\nu_{\text{opt}}^{\text{GHM}}$ in both SDBBP and HTP lets us directly compare the effects of different treatments of velocity-changing collisions on the line shapes via different kernels $\hat{M}$. Contrary to the hard-collision model of the HTP, the billiard ball kernel is based on the actual interaction potential, depends on the pertuber-to-absorber mass ratio, pre-collision velocity and the scattering angle, and has been shown previously to describe well the velocity-changing collisions of CO and Ar [29]. Eq. (13) is solved numerically in SDBBP, either with a simple diagonalization method [70] or with an iterative method [71].

Velocity-changing collisions interrupt the free molecular flow of the absorber and cause a reduction of the Doppler width. Additionally, they homogenize the speed distribution of the absorber, leading to a reduced influence of speed-dependent broadening and shift on the line-shapes [72]. In the two lowest pressures shown in Fig. 4, 10 Torr and 40 Torr, the dominant effect is the reduction of the Doppler width. The panels in Fig. 4 labeled qHTP–qSDBBP quantify the difference in modeling the Dicke effect by the two profiles. Despite a large difference between $\tilde{\nu}_{\text{VC}}$ values for the two lines, 19.5×10^{-3} cm^{-1}/atm for the P(8) line and 4.61×10^{-3} cm^{-1}/atm for the P(2) line, the amplitudes of line-shape profile differences are close to each for both lines. The large difference between these $\tilde{\nu}_{\text{VC}}$ values does not indicate the relative strength of the Dicke effect but it is an artifact of the adopted procedure for obtaining $\nu_{\text{opt}}^{\text{HTP}}(\nu_1)$ from $\nu_{\text{opt}}^{\text{GHM}}$, Eqs. (11), (12). Indeed, the parameter actually determining the degree of collisional narrowing in the HTP is $\text{Re}\,\nu_{\text{opt}}^{\text{GHM}}(\nu_1) = \nu_{\text{VC}} - \eta\Gamma(\nu_1)$, whose speed-averaged value is equal to 8.49×10^{-3} cm^{-1}/atm for the P(2) line and 9.99×10^{-3} cm^{-1}/atm for the P(8) line.

At the highest plotted pressure, 300 Torr, the Doppler width is completely reduced and the differences between qHTP and qSDBBP profiles are indicative of the strength of the competition between dephasing and velocity-changing collisions [72]. HTP is known to overestimate the effect of velocity-changing collisions and with the speed-dependent broadening in CO-Ar narrowing the lines, this should lead to the qHTP lines being broader than the qSDBBP lines. This effect is found to be negligible for the P(2) line and clearly visible for the P(8) line. The contrast between the lines is surprising, considering that the γ_2 values, see Table 1, and the $\langle \text{Re}\,\nu_{\text{opt}}^{\text{HTP}}(\nu_1)\rangle$ values are similar for both lines. We have found the reason for the excessive broadening to be the speed dependence of ν_{opt} introduced into the HTP by the η parameter. Evaluating the HTP with speed-independent ν_{opt} reduced the peak-to-peak differences for the P(8) line at 300 Torr to 0.13%.

Close analysis of the definition of ω_R reveals the interpretation of the η parameter within the GHM. The decomposition of ω_R given by Eq. (17) into two terms, one of them proportional to $\omega_0^{00}(q)$ and the other one to $\omega_1^{11}(q)$, comes from the fact that the ω_R collision integral is associated with the molecular velocity vector, which can be expressed as a combination of center-of-mass velocity and relative velocity vectors. The part associated with relative motion, viz. $(2/3)M_2\omega_1^{11}(q)$, is responsible for the velocity-changing contribution to the ω_R integral, whereas the part associated with center-of-mass motion, $M_1\omega_0^{00}(q)$, cannot contribute to velocity changes and it is responsible for the dephasing contribution [74,75]. Expressing $\nu_{\text{opt}}^{\text{GHM}}$, Eq. (10), in terms of $\Gamma_0 + \imath\Delta_0$,

$$\nu_{\text{opt}}^{\text{GHM}} = (2/3)nM_2(\omega_1^{11}(q))^* - M_2(\Gamma_0 + \imath\Delta_0), \tag{18}$$

and comparing it to Eq. (7) for $\nu_{\text{opt}}^{\text{HTP}}$, we can associate the HTP parameters ν_{VC} and η with the quantities defined within the quantum-mechanical GHM method. The frequency of velocity-changing collisions ν_{VC} corresponds to the complex conjugate of $(2/3)nM_2\omega_1^{11}(q)$ and the correlation parameter η to M_2. The GHM identification shows the $\eta = M_2$ parameter to be a purely kinetic factor, which is the same for all the lines for a given absorber-perturber pair and which does not account for all the correlation between velocity-changing and dephasing collisions. The GHM distinguishes a dephasing-only contribution in the form of $\omega_A = \Gamma_0 + \imath\Delta_0$ but no analogous velocity-changing-only contribution is defined, since both $\omega_1^{11}(q)$ and $\nu_{\text{opt}}^{\text{GHM}}$ also contain a dephasing contribution. It is worth noting that in the case of CO-Ar adopting the value of $M_2 = 0.59$ as that of η would lead to larger speed dependence of $\nu_{\text{opt}}^{\text{HTP}}(\nu_1)$, Eq. (7), and larger deviations of HTP high-pressure line shapes from SDBBP line shapes.

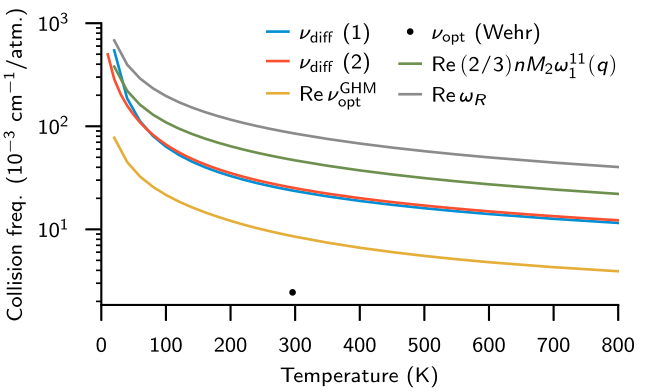

Fig. 5. Comparison between collision frequencies for the P(2) line: ν_{diff} (1) (blue), calculated from the classical model of Boushehri et al. [73] for the mass diffusion constant D; ν_{diff} (2) (red), based on quantum dynamics on isotropic part of the interaction potential [59]; $\text{Re}\,\nu_{\text{opt}}^{\text{GHM}}$ from Eq. (10) (yellow); ν_{opt} from Wehr's [29] SDBBP fits (black circle); the contribution to $\text{Re}\,\nu_{\text{opt}}^{\text{GHM}}$ from the $\omega_1^{11}(q)$ integral (green); the Re ω_R frequency from Eq. (17) (gray). (For interpretation of the references to colour in this figure legend, the reader is referred to the web version of this article.)

Similarly as in [32] for the H_2-He system, Fig. 5 presents the temperature dependence of the collision frequencies involved in describing the effects of velocity-changing collisions on spectral line shapes. ν_{diff} (1) is the velocity-changing collision frequency deduced from the mass diffusion coefficient D:

$$\nu_{\text{diff}} = \frac{\nu_p^2}{2D}, \tag{19}$$

for which the value of D was calculated based on the classical model and reference data of Boushehri et al. [73]. ν_{diff} (2) was obtained from quantum scattering calculation of momentum-transfer cross section on the isotropic part of the CO-Ar interaction potential [59] in the vibrational ground state, *i.e.* by evaluating Eq. (8) for CO treated as a structureless particle scattered by an isotropic potential. The ν_{opt} value (black circle) is the one obtained by Wehr et al. [29] from SDBBP fits to experimental data, labeled as ν in [29]. The GHM collision frequencies, $\text{Re}\,\nu_{\text{opt}}^{\text{GHM}}$, Re ω_R and $\text{Re}\,(2/3)nM_2\omega_1^{11}(q)$, were calculated as described in the current article. Contrary to the results for H_2-He [32–34], we see a clear difference between the plotted collision frequencies, illustrating that these are distinct quantities. Both Re ω_R and $\text{Re}\,(2/3)nM_2\omega_1^{11}(q)$ frequencies are significantly larger than ν_{diff} (1) and ν_{diff} (2), owing to both the small rotational constant of CO and anisotropy of

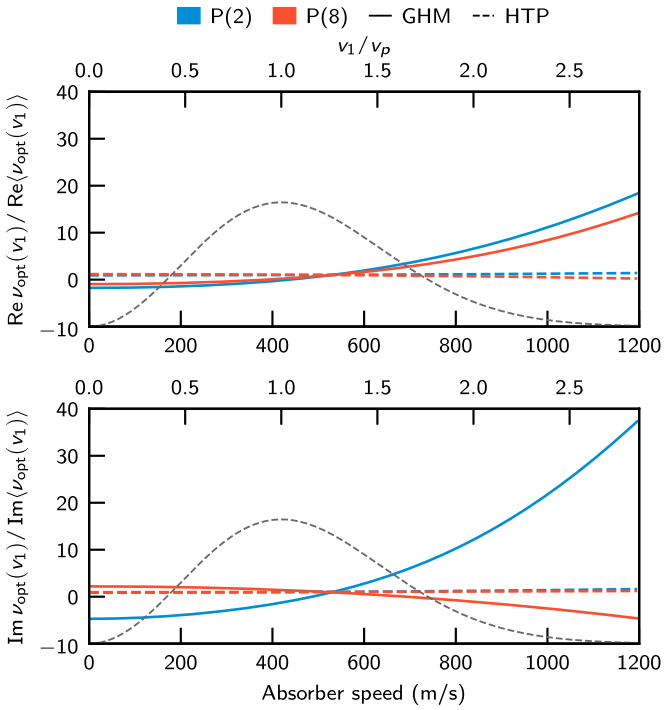

Fig. 6. Relative speed-dependence of GHM and HTP complex Dicke parameters at 296 K. Blue and red lines correspond to, respectively, P(2) and P(8) transitions. Solid lines show the values for $\nu_{opt}(v_1) \equiv \nu_{opt}^{GHM}(v_1)$, Eq. (21), and dashed lines for $\nu_{opt}(v_1) \equiv \nu_{opt}^{HTP}(v_1)$, Eq. (7). $\langle\nu_{opt}(v_1)\rangle$ is the Maxwell–Boltzmann speed average of the complex Dicke parameter with $\langle\nu_{opt}^{GHM}(v_1)\rangle = \langle\nu_{opt}^{HTP}(v_1)\rangle$. The Maxwell–Boltzmann speed distribution of CO at 296 K is shown as a gray dashed curve. (For interpretation of the references to colour in this figure legend, the reader is referred to the web version of this article.)

CO-Ar potential increasing the rate of collisional dephasing as compared to H_2-He. Compared to H_2-He, the CO-Ar colliding system is closer to various atmospheric molecular systems when considering rotational constant values and anisotropy of the interaction potential. As a consequence the presented conclusions are expected to hold for these systems also. The Re ν_{opt}^{GHM} frequency and ν_{opt} frequency obtained from SDBBP fits were found to be much smaller than ν_{diff}'s (see Fig. 5).

By analogy with the expression for speed-dependent broadening and shift, Eq. (5), we can formally define a speed-dependent collision integral $\omega_1^{11}(q; v_1)$ as [34]:

$$\omega_1^{11}(q; v_1) = \frac{\mu}{k_B T}\int_0^\infty v_r^3 \sigma_{\lambda=1}^q(E_{kin} = \mu v_r^2/2) f(v_r|v_1)\, dv_r, \qquad (20)$$

which can be used to define the speed-dependent $\nu_{opt}^{GHM}(v_1)$ as:

$$\nu_{opt}^{GHM}(v_1) = \frac{2}{3} n M_2 \omega_1^{11}(q; v_1)^* - M_2[\Gamma(v_1) + \imath\Delta(v_1)], \qquad (21)$$

which properly reduces to thermally-averaged ν_{opt}^{GHM} after integrating over absorber's speed distribution. Fig. 6 compares $\nu_{opt}^{GHM}(v_1)$ defined in Eq. (21) and $\nu_{opt}^{HTP}(v_1)$ defined in Eq. (7). The reason for the strong speed dependence of $\nu_{opt}^{GHM}(v_1)$ as compared to $\Gamma(v_1)$ or $\Delta(v_1)$, see Fig. 3, lies in the definition of the speed-dependent collision integral $\omega_1^{11}(q; v_1)$, which is independent of the specific molecular system under consideration. This is most apparent when comparing Re $\nu_{opt}^{GHM}(v_1)$ and $\Gamma(v_1)$ for the P(2) line. The cross section Re σ_1^1 involved in determining Re $\omega_1^{11}(q; v_1)$ and the cross section Re σ_0^1 involved in determining $\Gamma(v_1)$ are of similar magnitude for the P(2) line, see Fig. 1, but Re σ_0^1 cross section is weighted by v_r in Eq. (5) whereas Re σ_1^1 cross section is weighted by v_r^3 in Eq. (20). This is also the main factor causing the large difference between $\nu_{opt}^{HTP}(v_1)$, in which the speed-dependence is solely determined by the quantity $\eta(\Gamma(v_1) + \imath\Delta(v_1))$, and $\nu_{opt}^{GHM}(v_1)$. The speed dependence of $\nu_{opt}^{HTP}(v_1)$ is additionally reduced relative to $\nu_{opt}^{GHM}(v_1)$ because the value of η determined from Eq. (12) is smaller than that of M_2. A notable feature of Re $\nu_{opt}^{GHM}(v_1)$ at low absorber speeds seen in Fig. 6 is its negativity, which makes it difficult to assign an intuitive physical interpretation to the quantity.

It has been noted previously by Pine [2] within the framework of classical Boltzmann equation that evaluating profiles based on the hard-collision model with speed-dependent ν_{opt} invalidates the assumptions of the model, specifically the detailed balance for separate collision channels is not satisfied. Similarly, the ω_R parameter in the GHM is in general dependent on velocity, but the closed-form formula is obtained only when it is taken to be a speed-independent collision integral, see Eq. (17). Considering additionally the obvious failure of $\nu_{opt}^{HTP}(v_1)$ to reproduce the *ab initio* speed dependence, see Fig. 6, the incomplete accounting for correlations by the η parameter and the inconsistency between high-pressure HTP and SDBBP line shapes exacerbated by ν_{opt}'s speed dependence, it seems more reasonable to evaluate the HTP with ν_{VC} set to thermal average of the complex Dicke parameter ν_{opt}^{GHM} and η set to zero.

4.3. Quadratic speed dependence from temperature dependence

For a simple power-law dependence of pressure broadening and shift cross sections on relative speed (or collision energy), the thermally-averaged values of line-shape parameters and their speed dependence can be expressed analytically (see Appendix A) [67,68]. The resulting expressions can be manipulated to obtain approximate quadratic or hypergeometric speed-dependent parameters from the temperature dependence of averaged parameters, Eqs. (A.8), (A.9). These relations form the basis of the method proposed by Lisak et al. [37] to alleviate the problem of numerical correlation between Γ_2, Δ_2 and ν_{VC}, η in multispectrum fits [76]. In this method, Γ_2 and Δ_2 parameters are fixed in the fit to the approximate values to facilitate retrieval of accurate ν_{VC}, η values. We examine the agreement of such approximate parameters with the values obtained directly from the *ab initio* data. Fig. 7 shows the results of the comparison. Black lines show the reference γ_2 and δ_2 values obtained from applying Eq. (6) to the *ab initio* speed dependence. Blue lines show the results of applying Eq. (A.8) directly to the *ab initio* widths and shifts, representing the best-case scenario. Yellow lines show the more likely case, in which the temperature dependence is known from a fit of an analytical dependence to a set of points. For both γ_0 and δ_0, we used the approximate form adopted in the 2016 edition of the HITRAN database, *i.e.* linear for δ_0, Eq. (A.11), and power-law for γ_0, Eq. (A.10). Additionally, seeing that power-law dependence approximately matches the cross sections in Fig. 1 and the line-shape parameters in Fig. 2, which implies hypergeometric speed dependence, we have attempted a different method of arriving at quadratic-speed-dependent parameters. We have used Eq. (A.9) on *ab initio* temperature dependence to determine the parameter α describing hypergeometric speed dependence and evaluated the implied hypergeometric speed-dependence at $v_1 = v_p$ to obtain γ_2 and δ_2 from Eq. (6). The results are shown in red in Fig. 7.

The agreement between *ab initio*-derived speed-dependent parameters (black) and either one of two methods (blue and red curves) applied directly to *ab initio* temperature dependence does not consistently favor any one of them. The indirect hypergeometric method (red) shows excellent agreement in the case of P(2) line broadening, which matches the agreement of power-law fit to the broadening cross sections in Fig. 1, and converges to the *ab initio*-derived parameters at high temperatures. The same method

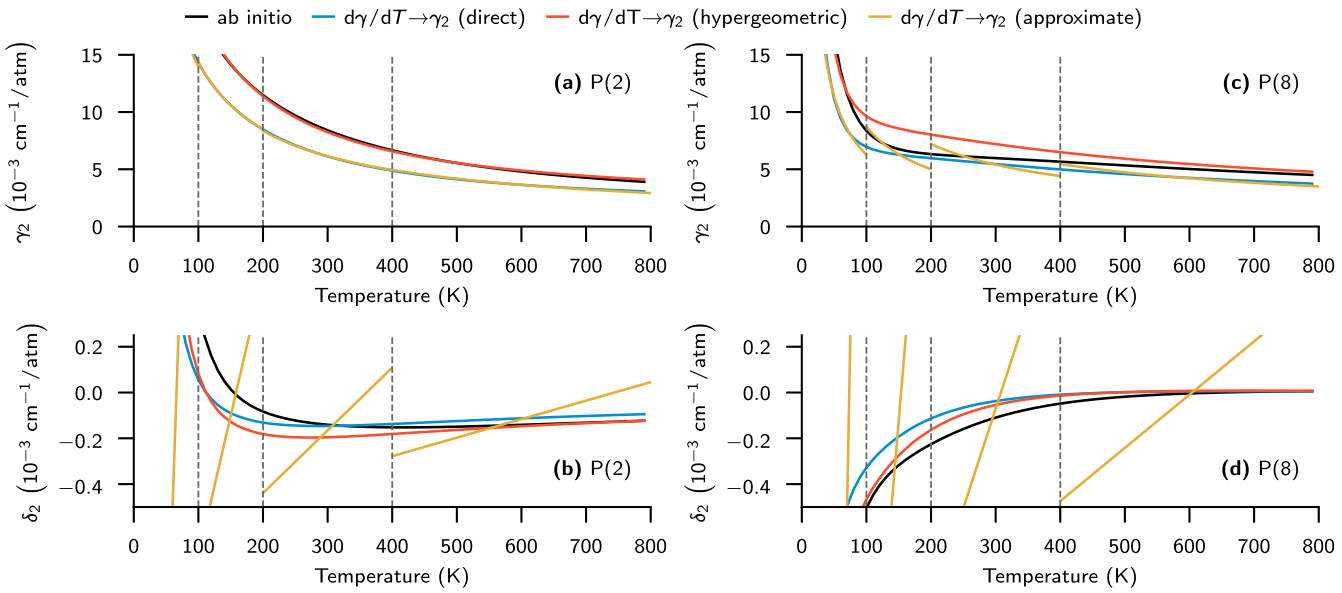

Fig. 7. Quadratic-speed-dependent coefficients obtained by: directly using Eq. (6) on *ab initio* speed-dependent widths and shifts (black); directly using Eq. (A.8) on *ab initio* temperature-dependent widths and shifts (blue); using Eq. (A.9) to obtain hypergeometric speed dependence from temperature dependence of *ab initio* widths and shifts and then using Eq. (6) on such speed dependence (red); using analytical formulas, Eqs. (A.10), (A.11), for temperature derivatives of approximate (exponential or linear) temperature dependence of widths and shifts (yellow). (For interpretation of the references to colour in this figure legend, the reader is referred to the web version of this article.)

applied to the P(8) line results in Γ_2 values differing by as much as 28% from *ab initio*-derived ones. On the other hand, direct differentiation (blue) offers better agreement with P(2) line shift and P(8) line broadening in the temperature range most easily accessible for laboratory measurements, but the P(2) line broadening is shifted by about 25% from the *ab initio*-derived values in the same temperature range. Speed-dependent shifts obtained from linear temperature dependence of pressure shifts (yellow) perform worse than a simple approximation by a constant value would, which provides an additional point in favor of the double-exponential model of Gamache and Vispoel [69,77].

The direct (blue and yellow) and indirect methods (red) assume that $\sigma_\lambda^q(E)$ cross sections are described by a square-root function, for the former, or a single power law, for the latter. These assumptions are fulfilled only to a limited degree for the CO-Ar lines shown here, as seen in Fig. 1. Examining $\sigma_\lambda^q(E)$ reported for other molecular systems, see Table 1 in [26] for references, we can expect these simple approximations to be inaccurate in other cases as well. Another indirect evidence for the cross sections not following a single power-law dependence is also given by a large improvement in accuracy when using the double-exponential model in modeling temperature dependence of γ and δ [69,77]. Nevertheless, despite their serious limitations, either of these simple methods we have evaluated can be useful in roughly estimating the importance of speed-dependent effects and providing initial guesses for a multispectrum fitting routine.

5. Conclusions

We have described and demonstrated a procedure for obtaining a full set of HTP line-shape parameters in a broad temperature range based on purely *ab initio* calculations utilizing an accurate interaction potential. A comparison with experimental data [27,30] has shown the accuracy of pressure broadening coefficients to be at sub-percent level and of pressure shift coefficients to be at 1%–3% level for the chosen two benchmark lines of CO perturbed by Ar. For the Dicke effect, this is the first *ab initio* calculation of ν_{opt} for a system exhibiting collision dynamics typical of Earth atmospheric species.

Based on the *ab initio* parameters, we examine the approximations of the HTP. In particular, we compare the quadratic and hypergeometric approximations of speed-dependence, finding no consistent improvement of one over another. We examine how discrepancies between *ab initio* and approximate $\Gamma(\nu_1)$ translate into actual line-shape residuals, finding small but significant deviations even when the approximated value of $\Gamma(\nu_1)$ deviates only by a few percent from the actual value. We examine the hard-collision model of velocity-changing collisions as adopted in the HTP. In particular, by comparing the HTP line shapes with SDBBP line shapes in different collisional regimes, we show that at high pressure the HTP overestimates the effect of velocity-changing collisions on the P(8) line shape. We provide the interpretation of ν_{VC} and η parameters in terms of GHM quantities and explain the large difference between speed dependence of ν_{opt} in HTP and GHM. We show that in contrast to H_2-He lines [32–34], for CO-Ar there is a substantial disagreement between mass transport and optical coherence transport coefficients. This behavior is also expected to occur for other atmospheric species with closely-lying rotational states. Finally, we examine the accuracy of the approximation schemes for temperature dependence of line-shape parameters adopted in the 2016 edition of the HITRAN database and the accuracy of a previously proposed scheme for deriving speed-dependent parameters from temperature dependence of averaged parameters. We find the approximate speed-dependent widths to be accurate within around 30% when obtained from power-law temperature dependence of pressure widths. In contrast, describing temperature dependence of pressure shifts by a linear function causes the approximate speed-dependent shifts to be up to a few tens of times larger in absolute value than the actual speed-dependent shifts.

The described procedure of obtaining the HTP line-shape parameters is directly applicable to other linear molecule-atom systems such as CO_2-Ar [78]. It can be extended in a straightforward manner to linear-linear systems [54], such as C_2H_2-N_2 [79], although the higher density of rotational states would make it necessary to use an approximate method [80] for the determination

of the S-matrix, such as the coupled states method [81], due to higher computational cost. The procedure will be further validated by performing calculations on other systems and comparing them with accurate experimental measurements. In particular, there are ongoing works on applying the GHM method to previously measured [82] second-overtone transitions of CO-Ar and to the more common diatom-diatom collisions represented by CO-N_2.

Declaration of Competing Interest

The authors declare that they have no known competing financial interests or personal relationships that could have appeared to influence the work reported in this paper.

CRediT authorship contribution statement

Grzegorz Kowzan: Conceptualization, Methodology, Software, Investigation, Funding acquisition, Writing - original draft, Writing - review & editing, Visualization. **Piotr Wcisło:** Conceptualization, Methodology, Software, Writing - original draft, Writing - review & editing. **Michał Słowiński:** Software, Investigation. **Piotr Masłowski:** Supervision, Funding acquisition. **Alexandra Viel:** Software, Investigation, Resources, Writing - original draft, Writing - review & editing. **Franck Thibault:** Conceptualization, Methodology, Software, Investigation, Resources, Writing - original draft, Writing - review & editing.

Acknowledgments

We thank prof. R. Ciuryło for fruitful discussions. This research was supported by National Science Centre, Poland project no. 2016/21/N/ST2/00334 and 2016/23/B/ST2/00730. G. K. was supported by National Science Centre, Poland scholarship 2017/24/T/ST2/00242. P. W. contribution is supported by National Science Centre, Poland through projects no. 2015/19/D/ST2/02195 and 2018/31/B/ST2/00720. M. S. contribution is supported by the National Science Centre, Poland through Project 2014/15/D/ST2/05281 and by the "A next-generation worldwide quantum sensor network with optical atomic clocks" project carried out within the TEAM IV Programme of the Foundation for Polish Science cofinanced by the European Union under the European Regional Development Fund. The project is supported by the French-Polish PHC Polonium program (project 42769ZK for the French part). The project is co-financed by the Polish National Agency for Academic Exchange under the PHC Polonium program (dec. PPN/X/PS/318/2018). The research is a part of the program of the National Laboratory FAMO (KL FAMO) in Toruń, Poland, and is supported by a subsidy from the Polish Ministry of Science and Higher Education.

Appendix A. Approximate temperature and speed dependence of line-shape parameters

In order to provide temperature dependence of line-shape parameters, the 2016 edition of the HITRAN database divides the whole temperature range into four subranges: 0 K–100 K, 100 K–200 K, 200 K–400 K, 400 K–∞ and assigns to each subrange a reference temperature: $T_{\mathrm{ref}}^{(1)} = 50$ K, $T_{\mathrm{ref}}^{(2)} = 150$ K, $T_{\mathrm{ref}}^{(3)} = 296$ K, $T_{\mathrm{ref}}^{(4)} = 400$ K. Values of γ_0 and δ_0 are provided at each reference temperature, which combined with $n_{\gamma_0}^{(i)}$ and $\delta_0'(i)$ coefficients can be used to approximate collisional broadening and shift at different temperatures with, respectively, power-law and linear functions:

$$\gamma_0^{(i)}(T) = \gamma_0\left(T_{\mathrm{ref}}^{(i)}\right)\left(T_{\mathrm{ref}}^{(i)}/T\right)^{n_{\gamma_0}^{(i)}}, \tag{A.1}$$

$$\delta_0^{(i)}(T) = \delta_0\left(T_{\mathrm{ref}}^{(i)}\right) + \delta_0'(i)\left(T - T_{\mathrm{ref}}^{(i)}\right), \tag{A.2}$$

Table A1
Power-law fit coefficients, Eq. (A.4), of spectroscopic cross sections from Fig. 1.

Line	Cross section	$\sigma_{\lambda,0}$ (Å^2/cm$^{-\alpha}$)	α
P(2)	$\mathrm{Re}(\sigma_{0,0}^1)$	356.4	−0.262
	$\mathrm{Re}(\sigma_{1,0}^1)$	389.5	−0.267
	$\mathrm{Im}(\sigma_{0,0}^1)$	5.77	−0.207
	$\mathrm{Im}(\sigma_{1,0}^1)$	4.16	−0.167
P(8)	$\mathrm{Re}(\sigma_{0,0}^1)$	251.0	−0.246
	$\mathrm{Re}(\sigma_{1,0}^1)$	447.2	−0.320
	$\mathrm{Im}(\sigma_{0,0}^1)$	70.6	−0.498
	$\mathrm{Im}(\sigma_{1,0}^1)$	51.9	−0.506

where the index i denotes the temperature range. The $\tilde{\nu}_{\mathrm{VC}}$ parameter is also approximated with a power law but based only on a single exponent κ, for the whole range and a reference value of $\tilde{\nu}_{\mathrm{VC}}$ at $T_{\mathrm{ref}}^{(2)}$:

$$\tilde{\nu}_{\mathrm{VC}}(T) = \tilde{\nu}_{\mathrm{VC}}\left(T_{\mathrm{ref}}^{(2)}\right)\left(T_{\mathrm{ref}}^{(2)}/T\right)^{\kappa}. \tag{A.3}$$

The temperature dependence of γ_2 and δ_2 is not explicitly modeled by HITRAN 2016, but the values of the parameters are provided at the four reference temperatures. The correlation parameter η is assumed to be temperature-independent and provided at $T_{\mathrm{ref}}^{(2)}$. The values of γ_0, n_{γ_0}, δ_0, δ_0', $\tilde{\nu}_{\mathrm{VC}}$ and κ for the P(2) line and P(8) line of CO-Ar are given in Table 1. In addition the supplementary material [dataset] [66] contains power-law coefficients for γ_2 (n_{γ_2}) and linear coefficients for δ_2 (δ_2') and η (η').

Power-law temperature dependence of line-shape parameters can be obtained by assuming power-law form of spectroscopic cross sections,

$$\sigma_\lambda^q(E_{\mathrm{kin}}) = \sigma_{\lambda,0}^q E_{\mathrm{kin}}^{\alpha}. \tag{A.4}$$

For the P(2) line of CO-Ar fundamental band, Wehr et al. [28] has previously obtained fit parameters $\mathrm{Re}(\sigma_{0,0}^1) = 361$ Å^2/cm$^{-\alpha}$ and $\alpha = 0.250$. The difference between these values and ours, shown in Table A.1, mostly comes from the different values of collision energy at which the fit was cut off, which was $E_{\mathrm{kin}} = 10$ cm^{-1} for [28] and $E_{\mathrm{kin}} = 50$ cm^{-1} for our fit.

Evaluating analytically the Boltzmann integrals from Eqs. (4), (9) with spectroscopic cross sections obeying the power law, Eq. (A.4), we obtain [67,68]:

$$\Gamma_0(T) = n\sigma_{\lambda,0}^q k_B^{\alpha+1/2}\sqrt{\frac{8}{\pi\mu}}\widetilde{\Gamma}(\alpha+2)T^{\alpha+1/2}, \tag{A.5}$$

where $\widetilde{\Gamma}$ is the gamma function. The exponent α is related to the temperature-dependence exponent n_{γ_0} from Eq. (A.1) by $\alpha = 1/2 - n_{\gamma_0}$ and to the exponent n from Ref. [37] by $\alpha = (n-1)/2$. Similarly, for speed-dependent parameters evaluating Eq. (5) for power-law cross section results in [14,49,67]:

$$\Gamma(v_1;T) = \frac{\Gamma_0(T)}{(\beta+1)^{\alpha+1/2}}\,\mathrm{M}\left(-\alpha-1/2, \frac{3}{2}, -\beta\frac{v_1^2}{v_p^2}\right), \tag{A.6}$$

where M is the confluent hypergeometric function [83, Sec. 13.2] and $\beta = m_2/m_1$. The commonly used quadratic speed dependence [84] can be obtained for $\alpha = 1/2$ [83, Eq. 13.2.2]:

$$\Gamma(v_1;T) = \Gamma_0(T) + \Gamma_2(T)\left(\frac{v_1^2}{v_p^2} - \frac{3}{2}\right), \tag{A.7}$$

implying unphysical kinetic energy square-root law for cross sections.

The preceding relations, Eqs. (A.5) and (A.7), can be used to derive quadratic and hypergeometric speed-dependent parameters from temperature dependence of Γ_0 and Δ_0 [37]. The Γ_2 (or Δ_2)

parameter is given by:

$$\Gamma_2(T) = \zeta T \frac{\mathrm{d}\Gamma_0(T)}{\mathrm{d}T}, \tag{A.8}$$

where $\zeta = (2/3)\beta/(1+\beta)$, and α exponent is given by:

$$\alpha(T) = \frac{T}{\Gamma_0}\frac{\mathrm{d}\Gamma_0(T)}{\mathrm{d}T} - \frac{1}{2}. \tag{A.9}$$

As applied to the form of temperature dependence adopted in the 2016 edition of the HITRAN databse, Eqs. (A.1), (A.2), this results in analytical formulas for quadratic speed-dependent width and shift:

$$\gamma_2^{(i)}(T) = \zeta(-n+1)\gamma_0\left(T_{\mathrm{ref}}^{(i)}\right)\left(T_{\mathrm{ref}}^{(i)}/T\right)^{n_{\gamma 0}^{(i)}}, \tag{A.10}$$

$$\delta_2^{(i)}(T) = \zeta\left[\delta_0\left(T_{\mathrm{ref}}^{(i)}\right) + \delta_0'(i)\left(2T - T_{\mathrm{ref}}^{(i)}\right)\right]. \tag{A.11}$$

References

[1] Duggan P, Sinclair PM, Berman R, May AD, Drummond JR. Testing lineshape models: measurements for v=1–0 CO broadened by He and Ar. J Mol Spectrosc 1997;186(1):90–8. doi:10.1006/jmsp.1997.7420.

[2] Pine AS. Asymmetries and correlations in speed-dependent Dicke-narrowed line shapes of argon-broadened HF. J Quant Spectrosc Radiat Transfer 1999;62(4):397–423. doi:10.1016/S0022-4073(98)00112-5.

[3] Chaussard F, Michaut X, Saint-Loup R, Berger H, Joubert P, Lance B, et al. Collisional effects on spectral line shape from the doppler to the collisional regime: a rigorous test of a unified model. J Chem Phys 1999;112(1):158–66. doi:10.1063/1.480570.

[4] Dicke RH. The effect of collisions upon the doppler width of spectral lines. Phys Rev 1953;89(2):472–3. doi:10.1103/PhysRev.89.472.

[5] De Vizia MD, Castrillo A, Fasci E, Amodio P, Moretti L, Gianfrani L. Experimental test of the quadratic approximation in the partially correlated speed-dependent hard-collision profile. Phys Rev A 2014;90(2):022503. doi:10.1103/PhysRevA.90.022503.

[6] Campargue A, Karlovets EV, Kassi S. The 4-0 band of carbon monoxide by high sensitivity Cavity Ring Down spectroscopy near 8200 cm^{-1}. J Quant Spectrosc Radiat Transfer 2015;154:113–19. doi:10.1016/j.jqsrt.2014.12.011.

[7] Wójtewicz S, Masłowski P, Cygan A, Wcisło P, Zaborowski M, Piwiński M, et al. Speed-dependent effects and Dicke narrowing in nitrogen-broadened oxygen. J Quant Spectrosc Radiat Transfer 2015;165:68–75. doi:10.1016/j.jqsrt.2015.06.022.

[8] Sironneau VT, Hodges JT. Line shapes, positions and intensities of water transitions near 1.28 μm. J Quant Spectrosc Radiat Transfer 2015;152:1–15. doi:10.1016/j.jqsrt.2014.10.020.

[9] Hashemi R, Predoi-Cross A, Nikitin AV, Tyuterev VG, Sung K, Smith MAH, et al. Spectroscopic line parameters of $^{12}CH_4$ for atmospheric composition retrievals in the 4300–4500 cm^{-1} region. J Quant Spectrosc Radiat Transfer 2017;186:106–17. doi:10.1016/j.jqsrt.2016.03.024.

[10] Hayden Smith WM, Conner CP, Simon J, Schempp WV, Macy W. The H_2 4-0 S(0, 1, and 2) quadrupole features in Jupiter. Icarus 1989;81(2):429–40. doi:10.1016/0019-1035(89)90062-6.

[11] Galatry L. Simultaneous effect of doppler and foreign gas broadening on spectral lines. Phys Rev 1961;122(4):1218–23. doi:10.1103/PhysRev.122.1218.

[12] Nelkin M, Ghatak A. Simple binary collision model for Van Hove's $G_s(r, t)$. Phys Rev 1964;135(1A):A4–9. doi:10.1103/PhysRev.135.A4.

[13] Rautian SG, Sobel'man II. The effect of collisions on the doppler broadening of spectral lines. Soviet Physics Uspekhi 1967;9(5):701–16. doi:10.1070/PU1967v009n05ABEH003212.

[14] Berman PR. Speed-dependent collisional width and shift parameters in spectral profiles. J Quant Spectrosc Radiat Transfer 1972;12(9):1331–42. doi:10.1016/0022-4073(72)90189-6.

[15] Lance B, Blanquet G, Walrand J, Bouanich J-P. On the speed-dependent hard collision lineshape models: application to C_2H_2 perturbed by Xe. J Mol Spectrosc 1997;185(2):262–71. doi:10.1006/jmsp.1997.7385.

[16] Ciuryło R, Szudy J. Speed-dependent pressure broadening and shift in the soft collision approximation. J Quant Spectrosc Radiat Transfer 1997;57(3):411–23. doi:10.1016/S0022-4073(96)00078-7.

[17] Wcisło P, Ciuryło R. Influence of the interaction potential shape on the Dicke narrowed spectral line profiles affected by speed-dependent collisional broadening and shifting. J Quant Spectrosc Radiat Transfer 2013;120:36–43. doi:10.1016/j.jqsrt.2013.02.023.

[18] Boone CD, Walker KA, Bernath PF. Speed-dependent Voigt profile for water vapor in infrared remote sensing applications. J Quant Spectrosc Radiat Transfer 2007;105(3):525–32. doi:10.1016/j.jqsrt.2006.11.015.

[19] Tran H, Ngo NH, Hartmann JM. Efficient computation of some speed-dependent isolated line profiles. J Quant Spectrosc Radiat Transfer 2013;129:199–203. doi:10.1016/j.jqsrt.2013.06.015.

[20] Ngo NH, Lisak D, Tran H, Hartmann J-M. An isolated line-shape model to go beyond the Voigt profile in spectroscopic databases and radiative transfer codes. J Quant Spectrosc Radiat Transfer 2013;129:89–100. doi:10.1016/j.jqsrt.2013.05.034.

[21] Tennyson J, Bernath PF, Campargue A, Császár AG, Daumont L, Gamache RR, et al. Recommended isolated-line profile for representing high-resolution spectroscopic transitions (IUPAC Technical Report). Pure Appl Chem 2014;86(12):1931–43. doi:10.1515/pac-2014-0208.

[22] Gordon I, Rothman L, Hill C, Kochanov R, Tan Y, Bernath P, et al. The HITRAN2016 molecular spectroscopic database. J Quant Spectrosc Radiat Transfer 2017;203:3–69. doi:10.1016/j.jqsrt.2017.06.038.

[23] Lisak D, Cygan A, Bermejo D, Domenech JL, Hodges JT, Tran H. Application of the Hartmann-Tran profile to analysis of H_2O spectra. J Quant Spectrosc Radiat Transfer 2015;164:221–30. doi:10.1016/j.jqsrt.2015.06.012.

[24] Ngo NH, Hartmann J-M. A strategy to complete databases with parameters of refined line shapes and its test for CO in He, Ar and Kr. J Quant Spectrosc Radiat Transfer 2017. doi:10.1016/j.jqsrt.2017.01.031.

[25] Hartmann J-M, Boulet C, Robert D. Collisional effects on molecular spectra. laboratory experiments and models, consequences for applications. Amsterdam: Elsevier; 2008. ISBN 9780444520173.

[26] Hartmann J-M, Tran H, Armante R, Boulet C, Campargue A, Forget F, et al. Recent advances in collisional effects on spectra of molecular gases and their practical consequences. J Quant Spectrosc Radiat Transfer 2018;213(nil):178–227. doi:10.1016/j.jqsrt.2018.03.016.

[27] Luo C, Wehr R, Drummond JR, May AD, Thibault F, Boissoles J, et al. Shifting and broadening in the fundamental band of CO highly diluted in He and Ar: A comparison with theory. J Chem Phys 2001;115(5):2198–206. doi:10.1063/1.1383049.

[28] Wehr R, Vitcu A, Ciuryło R, Thibault F, Drummond JR, May AD. Spectral line shape of the $P(2)$ transition in CO-Ar: Uncorrelated *ab initio* calculation. Phys Rev A 2002;66(6):062502. doi:10.1103/PhysRevA.66.062502.

[29] Wehr R, Ciuryło R, Vitcu A, Thibault F, Drummond JR, May AD. Dicke-narrowed spectral line shapes of CO in Ar: Experimental results and a revised interpretation. J Mol Spectrosc 2006;235(1):54–68. doi:10.1016/j.jms.2005.10.009.

[30] Wehr R, Vitcu A, Thibault F, Drummond JR, May AD. Collisional line shifting and broadening in the fundamental P-branch of CO in Ar between 214 and 324 K. J Mol Spectrosc 2006;235(1):69–76. doi:10.1016/j.jms.2005.10.004.

[31] The parameter ν_{opt} has also been called previously the frequency of optical velocity-changing collisions or the optical frequency of velocity-changing collisions.

[32] Thibault F, Patkowski K, Żuchowski PS, Jóźwiak H, Ciuryło R, Wcisło P. Rovibrational line-shape parameters for H_2 in He and new H_2-He potential energy surface. J Quant Spectrosc Radiat Transfer 2017;202:308–20. doi:10.1016/j.jqsrt.2017.08.014.

[33] Jóźwiak H, Thibault F, Stolarczyk N, Wcisło P. Ab initio line-shape calculations for the S and O branches of H_2 perturbed by He. J Quant Spectrosc Radiat-Transf 2018;219(nil):313–22. doi:10.1016/j.jqsrt.2018.08.023.

[34] Martínez RZ, Bermejo D, Thibault F, Wcisło P. Testing the ab initio quantum-scattering calculations for the D_2-He benchmark system with stimulated raman spectroscopy. J Raman Spectrosc 2018;49(8):1339–49. doi:10.1002/jrs.5391.

[35] Wcisło P, Thibault F, Zaborowski M, Wójtewicz S, Cygan A, Kowzan G, et al. Accurate deuterium spectroscopy for fundamental studies. J Quant Spectrosc Radiat Transfer 2018;213:41–51. doi:10.1016/j.jqsrt.2018.04.011.

[36] Shapiro DA, Ciuryło R, Drummond JR, May AD. Solving the line-shape problem with speed-dependent broadening and shifting and with Dicke narrowing. I. Formalism. Phys Rev A 2001;65(1):012501. doi:10.1103/PhysRevA.65.012501.

[37] Lisak D, Cygan A, Wcisło P, Ciuryło R. Quadratic speed dependence of collisional broadening and shifting for atmospheric applications. J Quant Spectrosc Radiat Transfer 2015;151:43–8. doi:10.1016/j.jqsrt.2014.08.016.

[38] Wcisło P, Gordon IE, Tran H, Tan Y, Hu S-M, Campargue A, et al. The implementation of non-Voigt line profiles in the HITRAN database: H_2 case study. J Quant Spectrosc Radiat Transfer 2016;177:75–91. doi:10.1016/j.jqsrt.2016.01.024.

[39] Ciuryło R, Pine AS, Szudy J. A generalized speed-dependent line profile combining soft and hard partially correlated Dicke-narrowing collisions. J Quant Spectrosc Radiat Transfer 2001;68(3):257–71. doi:10.1016/S0022-4073(00)00024-8.

[40] For short we call dephasing collisions those phase- and state-changing collisions which affect the internal motion of the molecule and lead to broadening as well as to shifting of transitions. Such collisions can be both elastic and inelastic. In addition, we remind the reader that the classical Dicke effect is tied to the translational motion, which is related only to elastic collisions.

[41] Baranger M. Simplified quantum-mechanical theory of pressure broadening. Phys Rev 1958;111(2):481–93. doi:10.1103/PhysRev.111.481.

[42] Baranger M. Problem of overlapping lines in the theory of pressure broadening. Phys Rev 1958;111(2):494–504. doi:10.1103/PhysRev.111.494.

[43] Baranger M. General impact theory of pressure broadening. Phys Rev 1958;112(3):855–65. doi:10.1103/PhysRev.112.855.

[44] Fano U. Pressure broadening as a prototype of relaxation. Phys Rev 1963;131(1):259–68. doi:10.1103/PhysRev.131.259.

[45] Ben-Reuven A. Symmetry considerations in pressure-broadening theory. Phys Rev 1966;141(1):34–40. doi:10.1103/PhysRev.141.34.

[46] Ben-Reuven A. Impact broadening of microwave spectra. Phys Rev 1966;145(1):7–22. doi:10.1103/PhysRev.145.7.

[47] For absorption processes the sign convention is to take the negative of the imaginary part of a spectroscopic cross section, or equivalently to consider the cross section $\sigma_\lambda^q(j_b, j_a; e) = \sigma_\lambda^q(j_a, j_b; e)^*$. The same remark applies to the velocity-changing cross sections further in the text.

[48] Fitz DE, Marcus RA. Semiclassical theory of molecular spectral line shapes in gases. J Chem Phys 1973;59(8):4380–92. doi:10.1063/1.1680636.
[49] Pickett HM. Effects of velocity averaging on the shapes of absorption lines. J Chem Phys 1980;73(12):6090–4. doi:10.1063/1.440145.
[50] Tip A. Transport equations for dilute gases with internal degrees of freedom. Physica 1971;52(4):493–522. doi:10.1016/0031-8914(71)90161-3.
[51] Hess S. Kinetic theory of spectral line shapes. The transition between doppler broadening and collisional broadening. Physica 1972;61(1):80–94. doi:10.1016/0031-8914(72)90035-3.
[52] Tip A. A kinetic equation for dilute polyatomic gases. Phys Lett A 1969;30(3):147–8. doi:10.1016/0375-9601(69)90901-3.
[53] Snider RF, Sanctuary BC. Generalized Boltzmann equation for molecules with internal states. J Chem Phys 1971;55(4):1555–66. doi:10.1063/1.1676279.
[54] Monchick L, Hunter LW. Diatomic–diatomic molecular collision integrals for pressure broadening and Dicke narrowing: A generalization of Hess's theory. J Chem Phys 1986;85(2):713–18. doi:10.1063/1.451277.
[55] Corey GC, McCourt FR. Dicke narrowing and collisional broadening of spectral lines in dilute molecular gases. J Chem Phys 1984;81(5):2318–29. doi:10.1063/1.447930.
[56] Schaefer J, Monchick L. Line broadening of HD immersed in He and H_2 gas. Astron Astrophys 1992;265:859–68.
[57] Demeio L, Green S, Monchick L. Effects of velocity changing collisions on line shapes of HF in Ar. J Chem Phys 1995;102(23):9160–6. doi:10.1063/1.468864.
[58] Yutsis AP, Levinson IB, Vanagas VV. Mathematical apparatus of the theory of angular momentum. Jerusalem: Israel Program for Scientific Translations; 1962.
[59] Sumiyoshi Y, Endo Y. Three-dimensional potential energy surface of Ar–CO. J Chem Phys 2015;142(2):024314. doi:10.1063/1.4905268.
[60] Child MS. Molecular Collision Theory. Academic Press; 1974.
[61] Hutson JM, Sueur CRL. Molscat: a program for non-reactive quantum scattering calculations on atomic and molecular collisions. CoRR 2018.
[62] Manolopoulos DE. An improved log derivative method for inelastic scattering. J Chem Phys 1986;85(11):6425–9. doi:10.1063/1.451472.
[63] Alexander MH, Manolopoulos DE. A stable linear reference potential algorithm for solution of the quantum close-coupled equations in molecular scattering theory. J Chem Phys 1987;86(4):2044–50. doi:10.1063/1.452154.
[64] For convenient comparison with rovibrational energy level structure commonly given in cm^{-1}, we provide collision energies also in cm^{-1} through E/hc with c in cm/s.
[65] Havenith M, Schwaab GW. Attacking a small beast: Ar–CO, a prototype for intermolecular forces. Zeitschrift für Physikalische Chemie 2009;219(8):1053–88. doi:10.1524/zpch.2005.219.8.1053.
[66] Kowzan G., Wcisło P., Słowiński M., Masłowski P., Viel A., Thibault F. Spectroscopic cross sections and HTP line-shape parameters for CO-Ar 0–1 P(2), P(8) lines. Mendeley Data; 2019.
[67] Ward J, Cooper J, Smith EW. Correlation effects in the theory of combined doppler and pressure broadening—I. Classical theory. J Quant Spectrosc Radiat Transfer 1974;14(7):555–90. doi:10.1016/0022-4073(74)90036-3.
[68] Lance B, Blanquet G, Walrand J, Populaire J-C, Bouanich J-P, Robert D. Inhomogeneous lineshape profiles of C_2H_2 perturbed by Xe. J Mol Spectrosc 1999;197(1):32–45. doi:10.1006/jmsp.1999.7892.
[69] Gamache RR, Vispoel B. On the temperature dependence of half-widths and line shifts for molecular transitions in the microwave and infrared regions. J Quant Spectrosc RadiatTransf 2018;217(nil):440–52. doi:10.1016/j.jqsrt.2018.05.019.
[70] Ciuryło R, Bielski A, Drummond JR, Lisak D, May AD, Pine AS, et al. High resolution studies on the influence of velocity hanging collisions on atomic and molecular line shapes. AIP Conf Proc 2002;645(1):151–60. doi:10.1063/1.1525447.
[71] Wcisło P, Cygan A, Lisak D, Ciuryło R. Iterative approach to line-shape calculations based on the transport-relaxation equation. Phys Rev A 2013;88(1):012517. doi:10.1103/PhysRevA.88.012517.
[72] Wcisło P, Thibault F, Cybulski H, Ciuryło R. Strong competition between velocity-changing and phase- or state-changing collisions in H_2 spectra perturbed by Ar. Phys Rev A 2015;91(5):052505. doi:10.1103/PhysRevA.91.052505.
[73] Boushehri A, Bzowski J, Kestin J, Mason EA. Equilibrium and transport properties of eleven polyatomic gases at low density. J Phys Chem Ref Data 1987;16(3):445–66. doi:10.1063/1.555800.
[74] Coombe DA, Snider RF, Sanctuary BC. Definitions and properties of generalized collision cross sections. J Chem Phys 1975;63:3015–30. doi:10.1063/1.431727.
[75] McCourt FRW, Liu W-K. Anisotropic intermolecular potentials and transport properties in polyatomic gases. Faraday Discussion Chem Soc 1982;73(nil):241. doi:10.1039/dc9827300241.
[76] Benner DC, Rinsland CP, Devi VM, Smith MAH, Atkins D. A multispectrum nonlinear least squares fitting technique. J Quant Spectrosc Radiat Transfer 1995;53(6):705–21. doi:10.1016/0022-4073(95)00015-D.
[77] Stolarczyk N, Thibault F, Cybulski H, Jóźwiak H, Kowzan G, Vispoel B, et al. Evaluation of different parameterizations of temperature dependences of the line-shape parameters based on ab initio calculations: case study for the HITRAN database. J Quant Spectrosc Radiat Transfer 2019;nil(nil):106676. doi:10.1016/j.jqsrt.2019.106676.
[78] Thibault F, Calil B, Buldyreva J, Chrysos M, Hartmann J-M, Bouanich J-P. Experimental and theoretical CO_2–Ar pressure-broadening cross sections and their temperature dependence. Phys Chem Chem Phys 2001;3(18):3924–33. doi:10.1039/B103625B.
[79] Thibault F, Corretja B, Viel A, Bermejo D, Martinez RZ, Bussery-Honvault B. Linewidths of C(2)H(2) perturbed by H(2): experiments and calculations from an ab initio potential. Phys Chem Chem Phys 2008;10(35):5419–28. doi:10.1039/b804306j. WOS:000258949000013
[80] Atom-molecule collision theory. Bernstein RB, editor. New York: Plenum Press; 1979.
[81] McGuire P, Kouri DJ. Quantum mechanical close coupling approach to molecular collisions. j_2-conserving coupled states approximation. J Chem Phys 1974;60(6):2488–99. doi:10.1063/1.1681388.
[82] Kowzan G, Stec K, Zaborowski M, Wójtewicz S, Cygan A, Lisak D, et al. Line positions, pressure broadening and shift coefficients for the second overtone transitions of carbon monoxide in argon. J Quant Spectrosc Radiat Transfer 2017;191:46–54. doi:10.1016/j.jqsrt.2016.12.035.
[83] NIST Digital Library of Mathematical Functions. http://dlmf.nist.gov/, Release 1.0.18 of 2018-03-27. F. W. J. Olver, A. B. Olde Daalhuis, D. W. Lozier, B. I. Schneider, R. F. Boisvert, C. W. Clark, B. R. Miller, and B. V. Saunders, eds. http://dlmf.nist.gov/;
[84] Priem D, Rohart F, Colmont J-M, Wlodarczak G, Bouanich J-P. Lineshape study of the j=3 ← 2 rotational transition of CO perturbed by N_2 and O_2. J Mol Struct 2000;517–518:435–54. doi:10.1016/S0022-2860(99)00268-9.